Cobalamin and microbial plankton dynamics along a coastal to offshore transect in the Eastern North Atlantic Ocean

Vanessa Joglar*[1,2], X.A. Álvarez-Salgado[3], Ana Gago-Martinez[4], Jose M. Leao[4], Clara Pérez-Martínez[5], Benjamin Pontiller[5], Daniel Lundin[5], Jarone Pinhassi[5], Emilio Fernández[1,2], Eva Teira[1,2]

[1] Centro de Investigación Mariña da Universidade de Vigo (CIM-UVIGO)

[2] Departamento Ecoloxía e Bioloxía Animal, Universidade de Vigo, Campus Lagoas-Marcosende, Vigo, 36310, Spain

[3] CSIC, Instituto de Investigacións Mariñas, Eduardo Cabello 6, Vigo, 36208, Spain

[4] Food and Analytical Chemistry Department, Chemistry Faculty, Department of Analytical and Food Chemistry, University of Vigo, Campus Universitario de Vigo, 36310 Vigo, Spain

[5] Centre for Ecology and Evolution in Microbial Model Systems – EEMiS, Linnaeus University, Stuvaregatan 4, 39231 Kalmar, Sweden

*Correspondence to: Vanessa Joglar

Novo CACTI Lab.100
Campus As Lagoas-Marcosende
Universidad de Vigo
36310 Vigo
Spain

+34 986 818790

vanjoglar@gmail.com

Summary

Cobalamin (B12) is an essential cofactor that is exclusively synthesized by some prokaryotes while many prokaryotes and eukaryotes require an external supply of B12. The spatial and temporal availability of B12 is poorly understood in marine ecosystems. Field measurements of B12 along with a large set of ancillary biotic and abiotic factors were obtained during three oceanographic cruises in the NW Iberian Peninsula, covering different spatial and temporal scales. B12 concentrations were remarkably low (< 1.5 pM) in all samples, being significantly higher at the subsurface Eastern North Atlantic Central Water than at shallower depths, suggesting that B12 supply in this water mass is greater than demand. Multiple regression models excluded B12 concentration as predictive variable for phytoplankton biomass or production, regardless of the presence of B12-requiring algae. Prokaryote production was the best predictor for primary production, and eukaryote community composition was better correlated with prokaryote community composition than with nutritional resources, suggesting that biotic interactions play a significant role in regulating microbial communities. Interestingly, co-occurrence network analyses based on 16S and 18S rRNA sequences allowed the identification of significant associations between potential B12 producers and consumers (e.g Thaumarchaeota and Dynophyceae, or *Amylibacter* and *Ostreococcus,* respectively), which can now be investigated using model systems in the laboratory.

Key words: Vitamin B12, interactions, community composition, NW Iberian Peninsula.

Introduction

Cobalamin (B12) is an essential coenzyme involved in many important metabolic pathways (e.g methionine or nucleotide synthesis) (Marsh, 1999; Madigan *et al.*, 2005; Monteverde *et al.*, 2017). In addition, vitamin B12 (hereafter B12) may be an important growth factor for phytoplankton (Droop, 1957; Provasoli, 1963; Carlucci *et al.*, 1969; Haines and Guillard, 1974; Swift, 1980; Croft *et al.*, 2005, 2006; Sañudo-Wilhelmy *et al.*, 2014). Vitamin B12 is a tetrapyrrolic cofactor containing a central cobalt atom, with varying upper and lower axial ligands, resulting in several B12 analogs differing in metabolic functions and bioavailability (Banerjee, 1997; Banerjee and Ragsdale, 2003; Brown, 2005; Koutmos *et al.*, 2009). The active coenzymes methylcobalamin (MB12) and adenosylcobalamin (AB12), as well as the non-catalytically active (transitive) congeners cyanocobalamin (CB12) and hydroxycobalamin (HB12) result from differences in the upper axial ligand (Banerjee, 1997; Brown, 2005). MB12 is the active form of cobalamin that is used by organisms for the synthesis of methionine through the cobalamin-dependent methionine synthase (MetH) (Matthews *et al.*, 2003) and AB12 is the coenzyme for methylmalonyl-CoA mutase, which is an essential enzyme in the metabolism of odd-chain fatty acids (Marsh, 1999). MB12 and AB12 are considered as extremely photolabile and quickly degrade to HB12 when exposed to light (Juzeniene and Nizauskaite, 2013; Juzeniene *et al.*, 2015; Vaid *et al.*, 2018). The lower axial ligand of this molecule can also present diversity, with 5,6 dimethylbenzimidazole or adenine building, respectively, cobalamin or pseudocobalamin (Stupperich and Krautler, 1988; Watanabe *et al.*, 1999; Helliwell *et al.*, 2016; Heal *et al.*, 2017).

Compared to mineral nutrients and trace elements, much less is known about the spatial and temporal availability of B12 in marine ecosystems, despite the recognition that

many microbial plankton species require an exogenous source of B12 (Carlucci and Bowes, 1970; Croft *et al.*, 2005; Bertrand and Allen, 2012; Sañudo-Wilhelmy *et al.*, 2014; Paerl *et al.*, 2018). Dissolved B12 concentrations are typically very low (picomolar range) and display pronounced spatial and temporal variation in marine systems (Sañudo-Wilhelmy *et al.*, 2006, 2012; Panzeca *et al.*, 2009; Koch *et al.*, 2012; Heal *et al.*, 2014; Cohen *et al.*, 2017; Suffridge *et al.*, 2018). A few studies observed that intermediate-depth waters (~200–500 m) contain higher B12 levels than those above and below that depth (Menzel and Spaeth, 1962; Carlucci and Cuhel, 1977; Sañudo-Wilhelmy *et al.*, 2012). This spatial pattern is consistent with the "nutrient-like" behavior of B12 proposed by Karl, (2002), being consumed in surface waters and accumulated in subsurface waters.

It is important to note that, historically, liquid chromatography-mass spectrometry (LQ-MS) only detected CB12 in marine system surveys (Okbamichael and Sañudo-Wilhelmy, 2004; Sañudo-Wilhelmy *et al.*, 2006; Panzeca *et al.*, 2009). More recently, Heal *et al.* (2014) developed a method to simultaneously detect four B12 congeners, showing that HB12 was the more abundant form, representing ca. 78% of the total dissolved B12 in coastal waters. A similar contribution of HB12 was measured in the particulate pool by Heal *et al.* (2017) in oceanic waters. In contrast, the study by Suffridge *et al.* (2018) found out that HB12 contributes to *ca.* 20% of total dissolved B12 and 70% of total particulate B12.

Only selected prokaryotes are capable of *de novo* B12 synthesis, while many prokaryote and eukaryote microbial species require an external supply of B12 (Carlucci and Bowes, 1970; Haines and Guillard, 1974; Helliwell *et al.*, 2011; Bertrand and Allen, 2012;

Sañudo-Wilhelmy *et al.*, 2014; Paerl *et al.*, 2015). Some algae have adapted to overcome B12 limitation in the environment by using alternative enzymes (Bertrand *et al.*, 2013; Helliwell *et al.*, 2014), whereas others require B12 and depend on an exogenous source of this organic molecule (Bertrand *et al.*, 2012). It has been suggested that phytoplankton may obtain B12 through interactions with prototrophic bacteria (Haines and Guillard, 1974; Croft *et al.*, 2005; Amin *et al.*, 2012; Cooper and Smith, 2015). B12 is considered a key metabolite mediating the symbiotic relationships between B12-auxotrophic algae and heterotrophic bacteria (Croft *et al.*, 2005; Amin *et al.*, 2012; Cooper and Smith, 2015; Durham *et al.*, 2015). In this interaction, algae obtain the vitamin directly from B12-synthesizing bacteria which, in return, receive photosynthates (Croft *et al.*, 2005; Wagner-Döbler *et al.*, 2010; Grant *et al.*, 2014).

The NW Iberian coastal zone presents incised valleys called rías, which are intermittently fertilized as a result of spring-summer upwelling events favored by northerly winds along the shore (Wooster *et al.*, 1976; Blanton *et al.*, 1984; Gonzalez-Nuevo *et al.*, 2014). Seasonality accounts for only 30% of the total annual variability in the wind regime, with most of the variability being associated with events of shorter temporal scales (Álvarez-Salgado *et al.*, 2003). These upwelling events inject cold and nutrient-rich Eastern North Atlantic Central Water (ENACW) into the rías (Fraga, 1981; Gómez-Gesteira *et al.*, 2001; Barton *et al.*, 2015). During the autumn and winter, when high river flows are recorded, frequent downwelling episodes introduce nutrient-poor surface waters of the adjacent shelf into the rías (Álvarez-Salgado *et al.*, 2000). A recent study by Barber-Lluch *et al.* (2019) at a fixed shelf station off this area (stn 3 in Fig. 1A) showed a marked seasonal variability in the response of phytoplankton and bacteria to inorganic nutrient and/or B12 additions in surface waters, with phytoplankton

122 responding at the beginning and at the end of the productive period. A detailed
123 experimental study by Joglar *et al*. (2020) at a shelf and an oceanic station off this area
124 (stn 3 and stn 6 in Fig.1A) also revealed that phytoplankton and prokaryotes frequently
125 respond to B12 and/or B1 additions. Overall, the magnitude of positive responses in the
126 sampling area after external B12 inputs was relatively small (Barber-Lluch *et al.,* 2019;
127 Joglar *et al*., 2020), and the patterns of microbial responses appeared to be mostly
128 controlled by the prokaryote taxonomic composition (Joglar *et al.*, 2020).

129

130 The first few measurements of B12 availability in this area revealed consistently low
131 concentrations of this growth factor (< 2.7 pM of CB12+HB12) (Barber-Lluch *et al.*
132 2020; Joglar *et al.,* 2020). Nevertheless, the limited number of samples included in these
133 studies, together with the lack of concomitant measurements of microbial plankton
134 activity and diversity, precluded solid conclusions on the role of B12 in the dynamics of
135 the microbial plankton assemblage in this productive area.

136

137 Within this context, we conducted extensive fieldwork to explore B12 availability in the
138 coastal transition zone off the NW Iberian Peninsula covering, for the first time,
139 relevant spatial (cross-shelf and vertical) and temporal (daily and seasonal) scales. The
140 methodology could not be set up to accurately detect MB12 and AB12, and thus, total
141 B12 measured must be considered a conservative estimate of the total dissolved B12.
142 Furthermore, we combined B12 measurements with a detailed description of dissolved
143 inorganic nutrients and dissolved organic matter, phytoplankton and prokaryote biomass
144 and production, and microbial plankton community composition (based on partial 16S
145 and 18S rRNA gene sequences). Our general hypothesis was that dissolved B12

concentration influences the abundance, distribution, and activity of microbial plankton and contributes to the delineation of ecological niches in this productive area.

Results

Three oceanographic cruises were conducted in different seasons (February, April and August) in 2016. During the first day of each cruise, a cross-shelf transect was performed to assess the spatial variability of B12 concentration. In addition, during the next 7 days of each cruise, intensive sampling was carried out at a fixed coastal station to study the short-term variability of B12 and its connection with biotic and abiotic factors. It is important to note that the quantified B12 forms were CB12 and HB12, so hereafter B12 refers to the sum of these two forms.

Spatial variability

Thermohaline variables, nutrients, and chlorophyll a

Different hydrographic conditions were found in the cross-shelf transect during each cruise. In February, weak northerly winds and high precipitation prevailed prior to cross-shelf sampling (Fig. 1B, 1C). The surface water temperature was constant throughout the transect, slightly increasing from 13.5 ºC in coastal waters to 13.9 ºC in oceanic waters (Fig. 2A). The temperature in deep waters was also lower in the coast (11.6 ºC) than in the adjacent ocean (12.5 ºC). The homogeneous temperature in the water column implied that the upper mixed layer (UML) was deep, exceeding 100 m at several stations. The cold and nutrient-rich ENACW, which upper limit is defined by the isopycnal level of 27 kg m^{-3}, was detected at the bottom in all stations during the winter cruise.

Freshwater inputs of the rivers flowed out as a thin surface layer causing a slight halocline at 10 m depth in the coastal stations. Chl-*a* was generally low along the transect, ranging from 0.07 to 1.31 mg m^{-3} with the highest concentrations in the UML without a clear inshore-offshore pattern (Fig. 2C). Nutrient concentrations were in the range of 1.61-10.88 µM for DIN and 0.16-0.74 µM for HPO_4^{2-} (Fig. 2D and 2E). Nutrient (i.e. DIN and HPO_4^{2-}) concentrations increased with depth, being the highest at the bottom of the shelf station (stn 3). In contrast, vitamin B12 concentrations ranged from 0.19 to 0.97 pM and B12-hotspots were mostly distributed within the UML except at stn 3 where highest concentrations were measured at the bottom (50 m depth) (Fig. 2F).

The April cruise was mostly characterized by a moderate downwelling turned into upwelling at the end of the cruise (Fig. 1B). Temperature values varied slightly along the transect being highest at the surface (ca. 13.3 ºC) and gradually decreased in subsurface waters to values lower than 13 ºC (Fig. 2G). The salinity was homogeneous along the water column and along the transect except in the coastal station (stn 3). In the coastal station, a strong continental freshwater discharge resulted in a thin UML of low-density water (Fig. 2H). In April, Chl-*a* concentrations increased with respect to February within the UML and the subsurface layer (SSL), located between the UML and the ENACW. Chl-*a* concentrations ranged from 0.08 in stn 6 to 2.61 mg m^{-3} in surface waters in stn 3 (Fig. 2I). Nutrient concentrations were in the range of 1.12–9.72 µM for DIN and 0.12-0.49 µM for HPO_4^{2-} (Fig. 2J and K). B12 levels ranged from 0.12–0.91 pM being maximum below the UML throughout the transect, except at stn 4 (Fig. 2L). Stn 3 had the highest nutrient concentrations, associated with low salinity.

In August, the surface temperature ranged from 14.2 to 15.9 ºC dropping to 13 ºC at 20 m in stn 3. The 13 ºC isotherm progressively deepened westwards. The ascending trend of subsurface temperature, σ-t and nutrient concentrations isolines towards the coast, indicate the upwelling of ENACW (Fig. 2M). The surface salinity values were higher than 35.5 PSU along the transect, showing the negligible influence of the river discharge (Fig. 2N). The thermohaline structure revealed the typical summer upwelling, prevailing from day 1 to day 5 (Fig. 1C). Chl-*a* concentration was generally high in the upper 30 m in shelf waters, where values higher than 5 mg m^{-3} were found. A progressive decrease was observed from stn 3 (15.2 mg m^{-3}) to stn 6 (1.28 mg m^{-3}) (Fig. 2O). In August, nutrient levels were in the range of 0.12-11.0 µM for DIN and 0.02-0.68 µM for HPO_4^{2-} (Fig. 2P and 2Q). Nutrients were depleted in the upper 25 m of the water column, and a marked nutricline was visible along the transect. Below 25 m depth nutrients increased towards the ENACW layer where the highest concentrations were observed. B12 levels ranged from 0.15 to 0.92 pM and showed a distribution pattern similar to that of inorganic nutrients (Fig. 2R).

Despite the clear variation in hydrographic conditions in the cross-shelf section during the different sampling periods, there were no significant differences in mean B12 concentrations among stations (ANOVA; df = 3, 57; P = 0.254), months (ANOVA; df = 2, 57; P = 0.398) or water layers (UML, SSL, and ENACW) (ANOVA; df = 2, 57; P = 0.154) (Supporting Information Fig. S1). In contrast, mean NO_3^- and HPO_4^{2-} concentrations were significantly higher in stn 3 than in stn 4 (Bonferroni, $P = 0.006$), and 6 (Bonferroni, $P < 0.042$) and significantly higher in the ENACW than in UML

(Bonferroni, $P < 0.001$). However, no differences were observed between seasons (Supporting Information Fig. S1).

Temporal variability

To investigate potential temporal patterns in the coastal stn 3 off the Ría de Vigo, abiotic (dissolved vitamin B12, nutrients, and DOM) and biotic (phytoplankton and prokaryote biomass and production as well as microbial taxonomic composition using 16S and 18S rRNA gene amplicon sequencing) variables were sampled daily or every second day for one week at each cruise.

Thermohaline variables, nutrients, and dissolved organic matter

Precipitations before and at the beginning of the February cruise (Fig. 1C) caused a persistent surface halocline, and a narrow UML, at the coastal station (Fig. 3B). The vertical distribution of temperature (< 13 ºC), salinity (> 35.5 PSU), and density σ-t (> 27 kg m^{-3}) in February indicated the presence of ENACW below 50 m depth throughout the sampling period (Fig. 3A). The haline stratification was associated with the development of a phytoplankton bloom in February. Increasing levels of Chl-*a* were observed, reaching a maximum (10.5 mg m^{-3}) by the end of the cruise (Fig. 3C). Nutrient concentrations were in the range of 2.4–12.0 µM for DIN, 1.1–7.8 for DON, 0.17–0.74 µM for HPO_4^{2-} and 45–69 µM for DOC (Fig. 3D-G). Relatively high concentrations of DIN and HPO_4^{2-} were measured at UML, associated with low salinity, yet, the highest values were observed in the ENACW. In contrast, maximum DON concentration was observed at the subsurface layer. DOC concentration was high at the surface but decreased below 15 m. The surface water was depleted in B12 with

243 concentrations < 0.3 pM along, while the ENACW had higher B12 concentrations,
244 peaking at 1.5 pM (Fig. 3H).

245

246 The April cruise coincided with prevailing downwelling conditions, as shown by the
247 negative upwelling index (UI) (Fig. 1C), when seawater temperatures ranged from 12.5
248 (in the deep water) to 14.6 ºC (at the surface) (Fig. 3I). ENACW was not detected
249 during in April, with σ-t values < 27 kg m^{-3} reaching down to 80 m depth (Fig. 3I).
250 Surface salinity values ranged from 31 to 34.5 PSU due to the continental runoff
251 influence (Fig. 3J). Chl-*a* concentration ranged from 3 to 0.4 mg m^{-3} and decreased
252 towards the end of the sampling period (Fig. 3K). Progressive warming of the water
253 column was observed in this period, accompanied by a noticeable discharge of nutrient-
254 rich freshwater. Nutrient concentrations ranged between 0.4–14 μM for DIN, 3.6–6.9
255 μM for DON, 0.04–0.49 μM for HPO_4^{2-}, 57–102 μM for DOC and 0.15–0.9 pM for
256 B12. The highest concentrations of DIN and DOC were always measured at the first 20
257 m (Fig. 3L and 3O), showing an inverse relationship with salinity. Surface DIN and
258 HPO_4^{2-} concentrations were close to 14 μM and 0.5 μM, respectively. In the SSL,
259 nutrient concentrations were very low, particularly after day 3. DON concentration was
260 homogeneous in the water column with values close to 6 μM, (Fig. 3M). Interestingly,
261 B12 concentrations decreased throughout the sampling period, with values well below
262 0.2 pM in the whole water column at the end of the cruise (Fig. 3P).

263

264 Under the prevailing upwelling conditions found in August (Fig. 1B), surface salinity
265 values were higher than 35.2 PSU in the whole water column, indicating a negligible
266 influence of the river discharge (Fig. 3R). Surface seawater temperatures ranged from

13 to 15.1 ºC. ENACW was detected below 30 m throughout the whole cruise (Fig. 3Q). During the summer upwelling, Chl-*a* was high in the upper 20 m, decreasing from 15.2 to 2.2 mg m^{-3} by the end of the cruise (Fig. 3S). Nutrient levels were in the range of 0.3-11.4 µM for DIN, 2.0–5.2 for DON, 0.1-0.79 µM for HPO_4^{2-}, 51–82 for DOC and 0.12–0.92 pM for B12. In the upper 20 m of the water column DIN, HPO_4^{2-} and B12 levels were depleted, except DIN and HPO_4^{2-} at day 7 (Fig. 3T, 3V and 3X). A slight enrichment of organic nutrients (DON and DOC) was observed in surface waters, decreasing at day 7. Below 20 m depth, inorganic nutrients (DIN and HPO_4^{2-}) and B12 increased towards the bottom.

Vitamin B12 concentration did not vary among the three sampling periods (ANOVA; df = 2, 59; $P = 0.679$) (Supporting Information Fig. S2). However, there were significant differences between water layers at the coastal station (stn 3) (ANOVA; df = 2, 59; $P < 0.001$), with a significantly higher concentration [mean ± standard deviation (SD)] in the ENACW (0.66 ± 0.107 pM) than in the UML (0.29 ± 0.049) (Bonferroni, $P < 0.001$) and SSL (0.35 ± 0.03) (Bonferroni, $P = 0.002$) (Supporting Information Fig. S2). Both, NO_3^- and HPO_4^{2-} followed a similar pattern to that of B12 at stn 3 (Supporting Information Fig. S2). NO_3^- concentrations differed between layers (ANOVA, $P < 0.001$), while HPO_4^{2-} differed between seasons (ANOVA; df = 2, 59; $P = 0.002$) and layers (ANOVA; df = 2, 59; $P < 0.001$). NO_3^- concentrations were higher in the ENACW (9.84 ± 0.39 pM) than in the UML (4.46 ± 0.72 pM) (Bonferroni, $P < 0.001$) and SSL (4.01 ± 0.45 pM) (Bonferroni, $P < 0.001$). HPO_4^{2-} concentrations showed seasonal variability with lower values in April (0.26 ± 0.024 pM) than in February (0.39 ± 0.039) (Bonferroni, $P = 0.069$) and August (0.44 ± 0.043 pM) (Bonferroni, $P = 0.003$). A principal component analysis (PCA) was conducted to visualize vertical and

292 temporal patterns of the abiotic factors in stn 3 (Fig. 4A). The PCA highlighted the
293 differences between sampling months (Fig. 4A). The first principal component
294 explained 45.7% of total variation of abiotic factors, and the second principal
295 component explained 15.9% of total variation of abiotic factors. NO_2^- and NH_4^+
296 explained most of the variation in April, pointing out to a relatively high relevance of
297 regeneration processes. In contrast, B12 and inorganic nutrients such as SiO_4^{4-}, HPO_4^{2-}
298 and NO_3^- were positively correlated with ENACW sampled in February and August
299 indicating new production associated with the upwelling event. Salinity was strongly
300 related to subsurface samples in February and temperature was mostly related to UML
301 samples in April and August. Considering all the abiotic variables there were significant
302 differences between months (ANOSIM, $P = 0.001$) and between layers (ANOSIM, $P =$
303 0.001).

304

305 *Size-fractionated phytoplankton and prokaryote biomass and production*

306 Nano- and microphytoplankton (cell size > 3 μm) dominated over picophytoplankton
307 (cell size < 3 μm) except in April when picophytoplankton dominated throughout the
308 sampling period (Fig. 5A). In February, an increase in both picophytoplankton biomass
309 (Chl-*a* < 3 μm) and nano-microphytoplankton biomass (Chl-*a* > 3 μm) was noticeable
310 in the second half of the cruise (Fig. 5A and 5B). Primary production (PP) increased in
311 parallel to Chl-*a* concentrations (Fig 5C and 5D). While picophytoplankton PP (PP < 3
312 μm) increased from 0.3 mg C m^{-3} h^{-1} at day 1 to 2.2 mg C m^{-3} h^{-1} at day 6 in surface
313 waters, nano-microphytoplankton PP (PP > 3 μm) increased from values close to 1 mg
314 C m^{-3} h^{-1} at the beginning of the cruise to 23 mg C m^{-3} h^{-1} at day 6 (Fig. 5C and 5D).
315 Total prokaryote biomass (PB) and heterotrophic prokaryote production (HPP)
316 decreased with depth (Fig. 5E and 5F). HPP ranged from 0.098 mg C m^{-3} h^{-1} in surface

317 waters to 0.015 mg C m^{-3} h^{-1} in the bottom, showing a slight increase in surface waters
318 towards the end of the cruise.

319

320 In April, Chl-*a* concentration was relatively low throughout the sampling period with
321 picophytoplankton as the main contributor to photosynthetic biomass (Fig. 5G). From
322 the third to the fifth day a slight increase in the picophytoplankton Chl-*a* up to 1.6 mg
323 m^{-3} was observed, while the maximum nano-microphytoplankton Chl-*a* was 1.4 mg m^{-3},
324 on day 1. A similar pattern was observed for PP, showing a peak of PP < 3 µm (2.5 mg
325 C m^{-3} h^{-1}) in surface waters on day 4 (Fig. 5I). On the other side, PP > 3 µm remained
326 lower than 5 mg C m^{-3} h^{-1} even at the surface (Fig. 5J). PB in April was higher than
327 during the phytoplankton bloom in February (Fig. 5K). HPP values were low and
328 similar to those measured in February, ranging between 0.4–0.1 mg C m^{-3} h^{-1} (Fig. 5L).

329

330 During the August cruise, the influence of upwelling was reflected in Chl-*a* > 3µm,
331 which showed a high concentration (17.5 mg m^{-3}) at surface waters at the beginning of
332 the cruise (Fig. 5N). The PP < 3 µm was close to 1 mg C m^{-3} h^{-1} at the surface while PP
333 > 3 µm was substantially high, reaching values up to 40 mg C m^{-3} h^{-1} (Fig. 5O and 5P).
334 In the top 20 m, PB and HPP reached ~60 mg C m^{-3} and 2.5 mg C m^{-3} h^{-1}, respectively
335 (Fig.5Q and 5R). These values gradually decreased from day 5 when upwelling
336 intensity decreased (Fig. 1B).

337

338 Chl-*a* concentrations [mean ± standard deviation (SD)] were significantly lower in
339 February (1.66 ± 0.41 mg m^{-3}) and April (1.43 ± 0.15 mg m^{-3}) than in August (4 ± 0.95
340 mg m^{-3}) (Bonferroni, $P = 0.033$), while PB was lower in February (1.19 mg C m^{-3}) than

in April (5.8 ± 0.5 mg C m^{-3}) (Bonferroni, P = 0.000) and August (11.8 ± 3.0 mg C m^{-3}) (Bonferroni, P = 0.000) (Supporting Information Fig. S2). As expected, PP was significantly higher during the summer upwelling (15.5 ± 3.4 mg C m^{-3} h^{-1}) (Bonferroni, P = 0.000), however HPP showed differences (ANOVA; df = 2, 81; P < 0.001 between the three seasons, being lowest in February (0.023 ± 0.005 mg C m^{-3} h^{-1}) and highest in August (0.48 ± 0.12 mg C m^{-3} h^{-1}) during the summer upwelling (Supporting Information Fig. S2).

The PCA of biological variables of stn 3 showed that while PP < 3 µm was linked to UML and SSL in February and April, PP >3 µm and HPP were strongly associated with the upwelling event in August. The two main components of PCA explained 89.8% of the total variation of biological variables (Fig. 4B). There were significant differences in the biotic variables between months (ANOSIM, P = 0.001) and layers (ANOSIM, P = 0.001) (Fig. 4B).

Relationship between resources and microbial biomass and production

We conducted a multiple linear regression analysis to explore the relationship between microbial biomass and production and resource availability (Table 1). As we aimed at explaining phytoplankton and prokaryote biomass and production from nutritional resources, we used size-fractionated Chl-*a* and PP, bulk HPP, and PB as explained (i.e. dependent) variables, and dissolved inorganic nutrients, dissolved organic matter, and vitamin B12 concentrations as explanatory (i.e. independent) variables. We also included PB and HPP as explanatory variables to model photosynthetic biomass and production and additionally, total Chl-*a* and total PP to model PB and HPP, thereby

365 including the potential effect of the biotic interaction between autotrophs and
366 heterotrophs.

367

368 The resulting linear regression models explained more than 74% of variability of the
369 phytoplankton biomass (Chl-*a* < 3 µm, Chl-*a* > 3 µm and total Chl-*a*) and primary
370 production (PP < 3 µm, PP > 3 µm and total PP) and 65 and 81% of the PB and HPP,
371 respectively.

372

373 Multiple linear regression analysis indicated that although dissolved nutrients explained
374 a significant amount of the variability in Chl-*a* and PP, HPP was the most influential
375 variable for total and large phytoplankton biomass and production (Table 1). Similarly,
376 total PP had a strong influence on PB and HPP. Strikingly, B12 concentration only
377 significantly influenced PB.

378

379 *Microbial community structure*

380 The microbial community composition did not show pronounced differences between
381 samples, and samples tended to cluster by water mass and by sampling month (Fig. 6).
382 The class Flavobacteria clearly dominated in the UML and SSL, mostly in April and
383 August. Archaea (mostly belonging to the Thaumarcheota phylum) and the marine
384 alveolata groups (MALV) dominated the ENACW and the SSL in February (Fig. 6).
385 *Synechococcus*, Rhodobacterales, *Polaribacter*, *Ostreococcus*, *Micromonas*,
386 Bacillariophyta, and fungi were systematically more abundant in the UML and SSL,
387 showing very low abundances in the ENACW. In April, a well-defined microbial

388 community shift occurred between days 1-3 and days 5–7 in the UML and SSL.
389 *Ostreococcus* dominated the phytoplankton community during day 1 and 3, and
390 *Synechoccocus*, *Thalassiosira* and other diatoms during day 5 and 7. The bacterial
391 groups *Amylibacter* and Oceanospirillales were more abundant during day 1 and 3 than
392 during day 5 and 7. The SAR11 clade was important during February in the UML and
393 SSL. Dinophyceae were relatively more abundant in summer.

394

395 The major microbial taxa were grouped into 3 different clusters depending on their
396 correlations with B12 and nutrient variables (Fig. 7). Cluster A (i.e. Archaea,
397 Oceanospirillales, SAR11, Dinophyceae, and MALV) correlated positively with
398 inorganic nutrients (e.g. HPO_4^{2-}, DIN, and NO_3^-), but negatively with NH_4^+, NO_2^- and
399 organic nutrients (i.e. DOC and DON). This cluster showed significantly positive
400 Pearson correlation coefficients ($P < 0.01$) with B12 concentrations. An opposing
401 pattern was found for cluster C (i.e. *Ascidiaceihabitans, Amylibacter, Micromonas,*
402 *Ostreococcus, Synechococcus,* fungi, and *Planktomarina)* (Fig. 7). A significantly
403 negative correlation with B12 concentration was observed in *Planktomarina* (R = -0.34,
404 $P = 0.009$) and *Synechococcus* (R = -0.34, $P = 0.009$). This cluster showed a strong
405 negative correlation with inorganic nutrients, especially the *Planktomarina* bacteria, and
406 fungi, which had a particularly strong correlation with DON. A third cluster,
407 characterized by weak positive or negative correlations with nutrients, included
408 Ciliophora, Rhodobacterales, Flavobacteria, *Polaribacter*, *Skeletonema, Thalassiosira,*
409 and other Bacillariophyta. The strongest negative (R = -0.43, $P = 0.001$) correlation
410 with B12 was found for other Bacillariophyta (cluster B in Fig. 7). A Mantel test
411 revealed a weak but significant relationship between prokaryote community structure
412 (mostly composed of heterotrophs) and resources (R = 0.17, $P = 0.002$) and between

413 eukaryote community structure (mostly composed of autotrophs) and resources (R =
414 0.14, P = 0.01). Interestingly, a significant relationship appeared between prokaryotes
415 and eukaryotes after correcting the effect of resources on both prokaryote and eukaryote
416 communities (R = 0.41, P = 0.002). Both microbial compartments were more related
417 among them than with resources.

418

419 *Co-occurrence networks*

420 In order to explore the potential interactions between major prokaryote and eukaryote
421 populations in the three different water layers, we examined the co-occurrence patterns
422 among the 50 most abundant amplicon sequence variants (ASVs) (25 eukaryotes and 25
423 prokaryotes) in each layer. From the 50 eligible nodes, 48 were included in UML and
424 SSL networks and 35 were included in the ENACW network (Fig. 8, Table 2). SSL and
425 ENACW networks were formed by only one component suggesting strong connectivity
426 between nodes (ASVs) below the UML. In contrast, 8 connected components composed
427 the UML network pointing out to a weak connectivity between ASVs at the surface.
428 Clustering coefficients (CL) were significantly higher than in random networks of the
429 same size (t-test, P = 0.001), whereas there were no significant differences between the
430 characteristic path lengths (CPL) and the random networks (CPLr). The considerably
431 higher CL of real versus random networks (CL/CLr > 2) is coherent with "small word"
432 network properties. The number of significant associations (edges), clustering
433 coefficients, the average number of neighbors and connectance, increased with depth
434 (UML < SSL < ENACW) (Table 2). Positive and negative co-occurrences in the built
435 networks are those where the two involved species coexist more and less frequently
436 than randomly expected, respectively (Veech, 2013). The proportion of negative co-
437 occurrences, potentially reflecting either niche partitioning or negative interactions, was

fairly similar in UML and SSL, 43 and 50% respectively, while in the ENACW most of the interactions were positive, with only 33% of negative associations. In the UML, a *Tenacibaculum* (Flavobacteriales) and a *Lonktanella* (Rhodobacterales) ASV showed many negative co-occurrences with *Ostreococcus* and other Prasynophyceae ASVs (Fig. 8A), while S*ynechococcus* showed positive co-occurrences with *Thalassiosira auguste-lienata, Chaetoceros tenuissimus,* and a fungal population (Fig. 8A). In the SSL, several *Amylibacter* ASVs showed positive co-occurrences with Dinophyceae, *Ostreococcus* and other Prasinophyceae ASVs (Fig. 8B). A large number of positive co-occurrences in the ENACW suggests overlapping niches and/or intense ecological interactions between Oceanospirillales or Thaumarchaeota and Dinophyceae, such as *Gyrodinium,* or Thoracosphaeraceae (Fig. 8C). In contrast, most negative associations involved Marine Alveolata ASVs (Fig. 8C).

Discussion

Cobalamin (vitamin B12) data were collected for the first time in the NW coast of the Iberian Peninsula covering relevant spatial and temporal scales. This multidisciplinary study revealed that CB12 and HB12 concentrations were lower than 1 pM in this ecosystem, which is consistent with a tight coupling between B12 producers and consumers.

S*patial and temporal distribution of B12*

The individual active MB12 and AB12 forms of B12 were not measured in our sampling area (Barber-Lluch *et al.* 2020), and thus the total B12 reported here is the sum of HB12 and CB12. Overall, B12 levels in the NW Iberian margin were very low

462 (Fig. 2 and 3) and showed relatively small zonal variation (Fig. 2). CB12 concentration
463 varied between undetectable and 0.77 pM, within the range of values observed in the
464 Pacific Ocean (< 0.25 pM) (Cohen *et al.*, 2017), in the upwelling area of San Pedro
465 Basin (Panzeca *et al.*, 2009) or in a Mediterranean-Atlantic Ocean transect (0.01–2.5
466 pM) (Suffridge *et al.*, 2018), although two orders of magnitude lower than CB12
467 concentrations observed along the California-Baja California margin (Sañudo-Wilhelmy
468 *et al.*, 2012). Overall, HB12 represented 91.1% of the total B12 measured in this study.
469 The highest HB12 concentration registered in this study was 0.97 pM, also within the
470 range observed in the Mediterranean (0.01–3.31 pM) (Suffridge *et al.*, 2018). In
471 contrast, Heal *et al.* (2014) found consistently higher HB12 concentrations throughout a
472 vertical profile in inshore Pacific waters (1.56–5.8 pM). Considering that the two active
473 forms (i.e. MB12 and AB12) have been described as photolabile (Juzeniene and
474 Nizauskaite, 2013; Juzeniene *et al.*, 2015; Vaid *et al.*, 2018), it could be expected that
475 their contribution to the total dissolved pool in surface waters should be small. The only
476 two studies measuring the four B12 congeners (MB12, AB12, HB12 and CB12)
477 reported disparate average contribution of HB12 to the total dissolved B12 pool,
478 representing ca. 20% in oligotrophic oceanic waters (Suffridge *et al*., 2018) and ca. 78%
479 in coastal waters (Heal *et al.*, 2014). Regardless of such differences, in both studies, the
480 contribution of the different B12 forms was relatively constant, which suggest that even
481 if we are underestimating the total B12 concentration, the variability patterns could be
482 taken as representative of those of total B12.

483

484 Compared with the relatively sharp spatial gradients observed in the North Pacific along
485 the California-Baja California margin (Sañudo-Wilhelmy *et al.*, 2012), we did not find
486 marked spatial patterns in the cross-shelf transects (Fig. 2). Although highly contrasted

areas were covered, Sañudo-Wilhelmy *et al.* (2012) found that areas of hundreds of kilometers where B12 concentration was nearly undetectable, probably because they only measured CB12. Our transect covered a less extensive area (Fig. 1) but both CB12 and HB12 were measured. Despite the lack of significant differences in B12 concentration along our transect (Supporting Information Fig. S1), higher values were found in coastal stations during April and August (Fig. 2). Higher B12 concentrations were observed within the UML in February, with the only exception of the innermost coastal station (Fig. 2). Spatial patches above the nutricline (the location of which frequently matches the UML limit) were also registered for B vitamins by Suffridge *et al.* (2018), coinciding with intense biological activity. When considering the temporal and vertical distribution of B12 at the innermost coastal station (stn 3) in February (Fig. 3 and 4), consistently higher B12 concentrations were found in the ENACW. On the other hand, B12 depletion was observed in the UML during the entire sampling period, regardless of the phytoplankton bloom development (Fig. 3 and 5). A similar pattern was observed in August when the biological activity was high and the concentrations of inorganic nutrients and B12 were the lowest in the surface and highest in the ENACW (Fig. 2). The positive correlation between B12, SiO_4^{4-}, NO_3^- and HPO_4^{2-} concentrations associated with the ENACW (Fig. 4) suggests that B12 follows a "nutrient-like" vertical distribution (Karl, 2002; Grant *et al.*, 2014), showing higher concentrations in intermediate water bodies (Sañudo-Wilhelmy *et al.*, 2012). We hypothesize that in this coastal location, B12 could be produced by prototrophic prokaryotes and accumulated in ENACW, transported to the photic zone through upwelling events or mixing processes, and rapidly consumed in the UML. The high relative abundance of Thaumarchaeota in ENACW (Fig. 6) supports this hypothesis, as this group seems to play a major role in B12 production in aquatic ecosystems (Doxey *et al.*, 2015; Heal *et*

512 *al.*, 2017). The vitamin B12 depletion observed in surface waters is also coherent with
513 B12 degradation upon exposure to solar radiation (Juzeniene and Nizauskaite, 2013).

514

515 A remarkably different B12 distribution occurred in April at the coastal station (Fig.
516 3P), when the prevailing southerly winds likely promoted the onshore transport of B12
517 depleted oceanic water, resulting in very low B12 levels from day 5 to 7 (Fig. 1, 2 and
518 3). The hypothesis of oceanic waters moving towards the innermost coastal station
519 during days 5–7 is supported by the warmer water column temperatures observed at the
520 end of the April sampling period (Fig. 3) and by changes in the microbial community
521 composition (Fig. 6), particularly by the relative increase of *Synechococcus,* which tend
522 to be dominant in oceanic waters in this sampling area (Teira *et al.*, 2009, Joglar *et al.*
523 2020). Interestingly, *Synechococcus* is a cyanobacteria that produces and uses
524 pseudocobalamin (Helliwell *et al.*, 2016), which was not measured in this study.

525

526 *The role of vitamin B12 in the dynamics of microbial plankton*

527 According to recent experimental studies conducted by our research group in this area,
528 ambient B12 could occasionally limit primary production, particularly at the beginning
529 of the productive period in early spring (Barber-Lluch *et al.*, 2019; Joglar *et al.*, 2020).
530 In addition, a positive correlation was found between depth-averaged Chl-*a* and
531 dissolved B12 concentrations in this sampling area (Barber-Lluch *et al.*, 2020). In
532 contrast, using an extensively larger dataset than that of Barber-Lluch *et al.* (2020), the
533 multiple regression analyses conducted here did not include B12 concentration as a
534 predictive variable for chlorophyll-*a* or primary production (Table 1). A lack of
535 correlation between phytoplankton and B12 could derive from the presence of non-

auxotrophic groups. However, the phytoplankton community was composed of many taxa that have been recognized to include B12-auxotrophs, such as Dinophyceae (Croft *et al.*, 2005; Tang *et al.*, 2010), or *Ostreococcus, Micromonas, Skeletonema,* or *Thalassiosira* (Swift, 1981; Croft *et al.*, 2005; Palenik *et al.*, 2007; Helliwell *et al.*, 2011; Ellis *et al.*, 2017; Cooper *et al.*, 2019), of which, only Dinophyceae abundance showed a positive correlation with B12 (Fig. 6 and 7). Multiple regression models for phytoplankton biomass and production included the concentration of NO_3^-, that was inversely related to phytoplankton, as significant explanatory variable (Table 1). Such negative relationships between primary producers and mineral nutrients have been previously observed, reflecting nutrient exhaustion during phytoplankton growth (Fisher *et al.*, 1992; Piehler *et al.*, 2004; Martínez-García *et al.*, 2010; Barber-Lluch *et al.*, 2019). Our findings thus contrast with similar studies in other coastal ecosystems characterized by higher ambient B12 levels (0.3–158 pM of CB12), where a significant and positive correlation was observed between CB12 and primary production rates (Koch *et al.*, 2011).

Regardless of the contribution of inorganic nutrients to explaining phytoplankton production and biomass, the variability explained by models including only nutrient variables was relatively low (Adjusted $R^2 < 0.48$), except for the biomass of picophytoplankton (Adjusted $R^2 = 0.79$) (Table 1). The fraction of variability explained by the models considerably increased when both nutrients and prokaryote-related variables (PB and HPP) were included (Adjusted $R^2 > 0.74$; Table 1), suggesting that prokaryote activity largely influenced phytoplankton growth. In the case of prokaryotes, only PB showed a positive relationship with the amount of dissolved vitamin B12 (Table 1), which is coherent with the fact that only prokaryotes have the capacity of *de novo* synthesizing this compound (Roth *et al.*, 1996; Martens *et al.*, 2002; Warren *et al.*,

2002). Suffridge *et al.* (2018) found that both CB12 and HB12 contributed to explaining the abundance of low nucleic acid bacteria in Atlantic waters. Interestingly, these authors did not find any significant correlation with the active forms AB12 and MB12, which were not detected in our study. Similarly, Gobler *et al.* (2007) also found a significant relationship between bacterial densities and CB12 concentration in coastal waters.

The lack of correlation between dissolved B12 concentration and phytoplankton variables could be caused by a rapid turnover rate of this growth factor in surface waters (Taylor and Sullivan, 2008), which is coherent with the constantly low concentration of B12 in the sampling area and the small-magnitude response of phytoplankton to experimental B12 additions (Barber-Lluch *et al.*, 2019; Joglar *et al.*, 2020), and suggest a tight coupling between production and consumption of this growth factor. The observed relationship between B12 and prokaryote biomass and the significant effect of heterotrophic prokaryote production on phytoplankton biomass and production (Table 1), is consistent with the hypothesis of phytoplankton B12 acquisition through interactions with bacteria, which may include intimate symbiotic relationships (Croft *et al.*, 2005; Amin *et al.*, 2012; Cooper and Smith, 2015; Seymour *et al.*, 2017). In such intimate interactions, B12 molecules appear to accumulate in bacterial membranes, and are rapidly assimilated by phytoplankton before being released into the environment (Amin *et al.*, 2012). If phytoplankton obtain B12 mostly from closely associated bacteria, then, changes in prokaryote community composition should have an impact on primary producers. A relatively strong and significant relationship was indeed found between eukaryote community composition, mostly dominated by phytoplankton taxa, and the prokaryote community composition. These observations point to the inclusion

586 of microbial interactions as a key piece in future studies of vitamin B12 dynamics in the
587 marine environment.

588

589 *Interactions between eukaryotes and prokaryotes as possible sources of B12.*

590 Recent experimental work demonstrated that dissolved B12 concentrations do not
591 provide enough information about the balance between B12 release by prokaryotes and
592 its consumption by prokaryotes and eukaryotes (Villegas-Mendoza *et al.*, 2019).
593 Therefore, despite its very low ambient concentration, we cannot disregard B12 as a
594 factor playing a significant role in microbial plankton dynamics in this coastal system.
595 We built co-occurrence networks for the different water layers to identify potential
596 biotic interactions between prokaryotes and eukaryotes that might involve B12 trading
597 (Fig. 8). The significant relationship found between prokaryote and eukaryote (mostly
598 phytoplankton) communities strongly suggests that biotic interactions might be playing
599 a critical role in the functioning of microbial communities in this coastal ecosystem.
600 Such dependence can involve phytoplankton-derived organic compounds required by
601 heterotrophic bacteria in exchange for nutrients or bacterial products required by
602 phytoplankton (Amin *et al.*, 2015; Durham *et al.*, 2015; Cirri and Pohnert,
603 2019)(Durham *et al.*, 2015).

604

605 The first study aimed at evaluating the interactions between algae and bacteria was
606 carried out in 1974, revealing that cultures with B12-producing bacteria enhanced
607 growth of B12-consuming algae (Haines and Guillard, 1974). There are many other
608 recent pieces of experimental evidence of biotic interactions between bacteria and
609 phytoplankton involving B12. For example, a vitamin B12-poor environment induces a

610 symbiotic relationship between *Lobomonas*, a B12-auxotroph green alga, and the
611 heterotrophic bacteria *Mesorhizobium* acting as the ultimate source of the vitamin
612 (Kazamia *et al.*, 2012). *Dinoroseobacter shibae*, a marine bacteria belonging to
613 Rhodobacterales, isolated from dinoflagellates (Biebl *et al.*, 2005) supplies B1 and B12
614 to its hosts in exchange for fixed carbon (Wagner-Döbler *et al.*, 2010), and *Ruegeria*
615 *pomeroyi* also provides B12 to the diatom *Thalassiosira pseudonana* in exchange for
616 organosulfurized compounds (Durham *et al.*, 2015).

617

618 The strong positive co-occurrences found in the ENACW involving Thaumarchaeota or
619 Oceanospirillales and dinoflagellates (Fig. 8C), suggests that these groups share
620 ecological niche, showing very similar correlations with resource variables, such as
621 inorganic nutrients or B12 (Fig. 7). It is important to note that co-occurrence does not
622 necessarily imply the existence of positive interaction, still, it has been demonstrated
623 that species that mutually benefit from each other tend to evolve towards ecological
624 niche convergence (Elias *et al.*, 2008). While many Dinophyceae have an absolute
625 requirement for exogenous B12 (Tang *et al.*, 2010; Koch *et al.*, 2014), both
626 Thaumarchaeota and Oceanospirillales have been reported to play an important role in
627 B12 biosynthesis within aquatic environments (Bertrand *et al.*, 2015; Doxey *et al.*,
628 2015), suggesting that these significant positive co-occurrences may involve B12
629 supply. Previous studies also suggested that the strong correlation between archaea and
630 phytoplankton found in marine systems could imply the archaeal supply of B12 to algae
631 (Rodionov *et al.*, 2003; Fietz *et al.*, 2011; Heal *et al.*, 2017). Furthermore, the
632 demonstration of the ability of bacteria to directly affect gene expression in some
633 Dinophyceae (Moustafa *et al.*, 2010; Gong *et al.*, 2017), suggests a close relationship
634 between these microbial planktonic groups.

635 In the subsurface layer, *Amylibacter* ASVs, belonging to the Rhodobacteraceae family,
636 and *Ostreoccocus* ASVs also appeared to coexist (Fig. 8B), sharing an ecological niche
637 (Fig. 7). It has been previously reported that *Ostreococcus* B12 requirements can be
638 provided by associated Rhodobacteraceae (Cooper *et al.*, 2019) Thus, the significant co-
639 occurrence observed might reflect a mutualistic interaction between *Amylibacter* and
640 *Ostreococcus* mediated by vitamin B12.

641

642 Competition among microbes for essential limiting nutrients is also common in marine
643 ecosystems. In the oceans, phytoplankton growth is often limited by the availability of
644 macronutrients such as nitrogen and phosphorus (Elser *et al.*, 1995; Joint *et al.*, 2002;
645 Lovdal *et al.*, 2008) or micronutrients such as iron or vitamins (Bertrand *et al.*, 2011;
646 Amin *et al.*, 2012; Koch *et al.*, 2012; Barber-Lluch *et al.*, 2019). Recent work point to
647 bacteria as a major sink of B12, potentially competing for this resource with
648 phytoplankton (Koch *et al.*, 2012; Heal *et al.*, 2017).

649

650 In the UML, significantly negative occurrences between *Tenacibaculum,* belonging to
651 Flavobacteriaceae, and the diatoms *Minidiscus* or *Thalassiosira* sp. were observed (Fig.
652 8A), suggesting competition-exclusion relationships. All currently sequenced
653 Flavobacteriaceae are predicted to be B12-auxotrophs (Sañudo-Wilhelmy *et al.*, 2014),
654 an trait also found in many diatoms (Croft *et al.*, 2006; Tang *et al.*, 2010; Bertrand and
655 Allen, 2012). As an example, *Thalassiosira* species have been reported of being B12-
656 dependent (Croft *et al.*, 2005; Sañudo-Wilhelmy *et al.*, 2014). Diatoms may increase
657 their cobalamin acquisition machinery in response to B12 scarcity (Bertrand and Allen,
658 2012), which may improve their competitiveness against auxotrophic bacteria for the

acquisition of B12. Interestingly, there were also some positive co-occurrences between *Synechococcus* ASVs and *Thalassiosira* or *Chaetoceros tenuissimus* ASVs. *Synechococcus* has been described as a major producer of pseudocobalamin, a chemical variant of B12 that can be remodeled by certain algae (Helliwell *et al.*, 2016; Heal *et al.*, 2017; Helliwell, 2017).

In summary, our results suggest that ambient B12 concentration *per se* does not contribute to ecological niche definition and does not appear to play a strong role in regulating microbial plankton dynamics in this upwelling system. Instead, heterotrophic prokaryote production appeared to be strongly related to phytoplankton biomass and primary production. The relatively high abundance of taxa previously described as B12-auxotrophs in this sampling area suggests that there might be a close balance between B12 production and consumption, which may result in low dissolved B12 concentrations. Interestingly, the co-occurrence analyses allowed the identification of interactions potentially involving B12 that can be subsequently tested with model systems in the laboratory. The fact that prokaryote and eukaryote taxonomic composition showed higher correlation between them than with nutritional resources, suggests that the biotic interactions between phytoplankton and prokaryotes may represent a predominant driving force of oceanic microbial community dynamics.

Experimental procedures

Survey area

The Ría de Vigo (NW Spain) is a coastal embayment and its main tributary into the innermost part of the Ría is the Oitabén-Verdugo River. This Ría is affected by

683 intermittent upwelling of cold and inorganic nutrient-rich subsurface water from April
684 to September and downwelling of warm and nutrient poor shelf surface water from
685 October to March. Despite this seasonality, short-term variability in the wind regime is
686 recurrent and significant in the area, with upwelling and downwelling events occurring
687 within each season (Figueiras *et al.*, 2002; Piedracoba *et al.*, 2005; Barton *et al.*, 2016).
688 The Ría de Vigo and its adjacent shelf is a highly productive and very dynamic coastal
689 system, where microbial community composition varies over short temporal and spatial
690 scales (Cermeño *et al.*, 2006).

691

692 **Field observations**

693 Field measurements were obtained during the 'ENVISION' cruises held in 2016 aboard
694 the R/V Ramón Margalef. Cruises were carried out in February, coinciding with the
695 spring bloom, in April under upwelling relaxation, and in August during the upwelling
696 event.

697

698 In order to describe the spatial variability, a total of 9 stations were occupied (Fig. 1A)
699 along a zonal transect of the Ría de Vigo from the inner continental shelf (42 ºN, 8.88
700 ºW) to open ocean waters on the shelf-break (42.142 ºN, 9.708 ºW) during the first day
701 of each cruise (day 1). At each station, vertical profiles of temperature and salinity were
702 recorded using a regular CTD-rosette sampler down to a maximum depth of 200 m.
703 Seawater samples for chemical and biological analyses were collected at 4 stations (stn
704 3, stn 4, stn 5 and stn 6), hereafter referred to as biological stations. Stn 3 and stn 4 are
705 considered as on-shelf stations since their depth is less than 200 m, being stn 3 closer to
706 the mouth of the Ría de Vigo. In contrast, the deeper stn 5 and 6 are considered as shelf-
707 break stations, with stn 6 being the most oceanic sampling point. Seawater samples for

708 vitamin B12, inorganic nutrients, and total chlorophyll *a* concentration were drawn from
709 5 depths at each station. In order to explore temporal variability, the on-shelf stn 3 (Fig.
710 1A) was visited daily from day 1 to day 7 during each cruise. This station was
711 intensively sampled for vitamin B12, inorganic nutrients and dissolved organic matter,
712 size-fractionated chlorophyll *a*, size-fractionated primary production, prokaryote
713 biomass and prokaryote heterotrophic production. The sampling depths were chosen
714 based on the vertical profiles of chlorophyll a fluorescence and temperature considering
715 the downward CTD casts.
716
717 Upwelling index (UI) was estimated from surface winds in a 2° x 2° cell centered at 42
718 °N, 10 °W. Daily UI values were computed by the Instituto Español de Oceanografía
719 (www.indicedeafloramiento.ieo.es) from sea level pressure fields over the ocean
720 supplied by the US Navy Operational Global Atmospheric Prediction System
721 (NOGAPS) model maintained by FNMOC (Fleet Numerical Meteorology and
722 Oceanography Center) (Gonzalez-Nuevo *et al.*, 2014). Precipitation data was
723 downloaded from the meteorological station Illas Cies (ID 10125) run by the Regional
724 Weather Forecast Agency-Meteogalicia (www.meteogalicia.gal).
725
726 **Size-fractionated chlorophyll *a* concentration**
727 Chlorophyll *a* (Chl-*a*) concentration was measured as a phytoplankton biomass proxy.
728 A volume of 300 mL of water samples were sequentially filtered through 3 and 0.2 μm
729 pore-size polycarbonate filters and frozen at -20 ºC until analysis. Chl-*a* from samples
730 was extracted with 90% (v/v) acetone (HPLC grade) at 4 ºC overnight in dark
731 conditions. Chl-*a* fluorescence was determined with a TD-700 Turner Designs
732 fluorometer calibrated with pure Chl-*a* standard solution.

733

734 **Size-fractionated primary production**

735 Size-fractionated photosynthetic carbon incorporation rates were estimated using ^{14}C-
736 sodium bicarbonate according to Marañón *et al.* (2001). In brief, 100 µL $NaH^{14}CO_3$
737 stock solution (126 µCi mL^{-1} specific activity) were added to seawater samples
738 transferred to acid-cleaned polycarbonate bottles. For each sample, three light and one
739 dark bottles were incubated for ~6 hours (typically from 11:00 to 17:00 h, local time)
740 under *in situ* irradiance and temperature conditions. At the end of the incubation,
741 samples were gently sequentially filtered through 3 µm and 0.2 µm pore-size Whatman
742 PC filters. Non-assimilated radioactive ^{14}C was removed by exposing the filters to 10%
743 (v/v) HCl for 12 hours and constant shaking. After decontamination of inorganic ^{14}C,
744 filters were transferred to scintillation vials to which 4 mL of scintillation cocktail
745 (Ultima Gold XR, Perkin Elmer) was added before measuring the radioactivity signal as
746 disintegrations per minute (DPM) in a Perkin Elmer TriCarb 3100 TR counter.

747

748 **Prokaryote biomass and production**

749 Unfiltered seawater samples (2 mL) for prokaryote biomass (PB) quantification were
750 preserved with 1% (v/v) paraformaldehyde + 0.05% (v/v) glutaraldehyde incubated for
751 20 min at room temperature and stored at -80 ºC after being flash-frozen with liquid
752 nitrogen.

753

754 The abundance of heterotrophic prokaryotes was determined using a FACSCalibur flow
755 cytometer equipped with a laser emitting at 488nm. Samples were stained with SYBR
756 Green DNA fluorochrome prior to analysis, and prokaryote abundance was detected by

their signature of side scatter (SSC) and green fluorescence as described by Gasol and Del Giorgio (2000). The empirical calibration between light side scatter (SSC) and cell diameter described by Calvo-Díaz and Moran (2006) was used to estimate the biovolume (BV) of cells. BV was converted into biomass by using the allometric factor of Norland (1993) (fg C $cell^{-1}$ = 120 × $BV^{0.72}$) for the coastal samples and using the open ocean conversion factor for the oceanic samples (fg C $cell^{-1}$= 350 × BV).

Heterotrophic prokaryote production (HPP) was measured following the ^{3}H-leucine incorporation method (Smith and Azam, 1992). Three replicates and two killed control of unfiltered seawater were sampled (1 mL). Samples were spiked with 40 µL leucine (47 µCi mL^{-1} specific activity stock solution) and incubated for 90 min in the same conditions as PP samples. Processed samples were analyzed in a Perkin Elmer TriCarb 3100 TR counter, and the HPP was calculated from the leucine uptake rates using a theoretical leucine to a carbon conversion factor of 3.1 kg C mol Leu^{-1} (Smith and Azam, 1992).

Inorganic and organic nutrients

Aliquots for inorganic nutrient determinations (ammonium, nitrite, nitrate, phosphate and silicate) were collected in first place and directly from the Niskin bottle in order to avoid contamination. 5% (v/v) HCl precleaned 50 mL polyethylene bottles were filled with the sample employing free-contamination plastic gloves and immediately frozen at –20 °C until analysis by standard colorimetric methods with an Alliance Futura segmented flow analyzer (Grasshoff *et al.,* 1999). The measurement error was 0.1 µmol L^{-1} for nitrate, 0.02 µmol L^{-1} for nitrite and phosphate and 0.05 µmol L^{-1} for

781 ammonium and silicate. Dissolved inorganic nitrogen (DIN) concentration was
782 calculated as the sum of the ammonium, nitrite and nitrate concentration.

783 Dissolved organic carbon (DOC) and total dissolved nitrogen (TDN) samples were
784 collected in 250 mL acid-washed all-glass flasks and were gently filtered through acid
785 rinsed 0.2 μm Pall Supor filters. Filtration was done in an acid-cleaned all-glass
786 filtration device under low pressure of high purity N_2. About 15 mL of the filtrate was
787 collected in pre-combusted (450 ºC for 24 h) Wheaton amber glass vials of 20 mL,
788 stopped with acid-cleaned PTFE lined caps and immediately frozen at -20 ºC until
789 simultaneous DOC and TDN analysis in the base laboratory. After defrosting, samples
790 were acidified with 150 μL of 25% (v/v) H_3PO_4 and analyzed in a Shimadzu TOC-V
791 analyzer coupled in series with a TNM-1 chemiluminescence detector. The
792 measurement error was 0.7 μmol L^{-1} for DOC and 0.3 μmol L^{-1} for TDN. Reference
793 materials provided by D. A. Hansell (University of Miami) were analyzed to check the
794 accuracy of the instruments. Dissolved organic nitrogen was obtained subtracting
795 ammonium, nitrite and nitrate to TDN.

796

797 **Vitamin B12**

798 Seawater samples (2 L) for dissolved vitamin analysis were taken at five depths in the
799 station closet to the coast (stn 3) on day 1, day 3, day 5 and day 7 of the cruise and in all
800 biological stations during the day 1 of the cruise. Samples were filtered through 0.2 μm
801 Sterivex filter units under dim light conditions, and frozen at -20 ºC until further
802 analysis. The methodology for concentration and detection of B12 was adapted from
803 Sañudo-Wilhelmy *et al.* (2012), Heal *et al.* (2014) and Suffridge *et al.* (2017) and is
804 fully described in Barber-Lluch *et al.* (2020). The pH of 1 L of water was adjusted to

6.5 and pre-concentrated using a solid-phase extraction (SPE) column (Econo-Pac® Chromatography Columns BioRad) with 20 mL bed volume filled with 5 g of HF-Bondesil C18 resin (Agilent Technologies) at a flow rate of 1 mL min^{-1}, avoiding light exposure. The B12 vitamin retained on stationary phase were eluted using 12 mL of methanol (MeOH) LCMS grade. The eluate was evaporated under nitrogen stream using N_2 gas Turbovap until obtain the final volume of 300 -500 µL of sample, and then was frozen at -20 ºC until analysis.

The analysis of dissolved vitamin B12 concentrations in water samples were carried out by LC-MS/MS, following the conditions described by Barber-Lluch *et al.* (2020). We analyzed two B12-forms; cyanocobalamin (CB12) and hydroxocobalamin (HB12), as we could not successfully set up the method for adenosylcobalamin (AB12) and methylcobalamin methylcobalamin (MB12) measurement. Both MB12 and AB12 standards were highly unstable during the analyses, rapidly converting to HB12, which precluded us to obtain an accurate calibration curve for these two congeners (see Barber-Lluch *et al.* 2020). It is important to note that photodegradation was minimized covering samples and lab materials with black opaque plastics. Briefly, quantification of dissolved B12 (HB12 and CB12) was carried out using an Agilent 1290 Infinity LC system (Agilent Technologies, Waghaeusel Wiesental, Germany), coupled to an Agilent G6460A triple quadrupole mass spectrometer equipped with an Agilent Jet Stream ESI source. The LC system used a C18 reversed-phase column Agilent Zorbax SB-C18 Rapid Resolution HT (2.1 × 50 mm, 1.8 µm) with a 10 µL sample loop. Mass Hunter Workstation software B.04.01 from Agilent Technologies was used for data acquisition and quantitative analysis. The mobile phase was (A) metanol and (B) wáter both LCMS grade and both buffered to pH 5.0 with 0.5% (v/v) of acetic acid (LCMS grade). The

chromatographic conditions consist in a isocratic condition of 7% of mobile phase B during 2 min, a gradient from 7 to 100% of mobile phase B were set up for the next 9 min, an isocratic condition with 100% B for 2.5 min and returning to initial conditions until completing 15 min of run. Limits of detection (LODs) and limits of quantification (LOQs) were determined using sequential dilutions of the lowest point of the calibration curves. LODs were defined as the lowest detectable concentration of the analyte with a signal-to-noise (S/N) ratio for the qualitative transition of at least 3. In the same way, LOQs were defined as the lowest quantificable concentration with a S/N ratio of 10 for the quantitative transition. The LODs obtained were 0.04 for hydroxocobalamin (HB12) and 0.01 pmol L^{-1} for cyanocobalamin (CB12), while the LOQs values were 0.05 and 0.025 pmol L^{-1} for HB12 and CB12, respectively. The relative standard deviation of triplicate injections was lower than 5% for both B12 congeners.

Standard of CB12 and HB12 were added in triplicate to a blank of seawater for recovery studies following the conditions described by Barber-Lluch *et al.* (2020) and the average B12 recovery percentage after pre-concentration and extraction of B-vitamin spiked samples was 93%.

Microbial community composition

DNA samples were taken in the coastal station (stn 3) during the three ENVISION cruises. In particular, sampling for microbial plankton community composition was carried out on day 1, day 3, day 5 and day 7 at 5 different depths from surface to 80 m depth. 2 L water samples were sequentially filtered through 3 μm pore size polycarbonate filters and 0.2 μm pore size Sterivex Filter Units and immediately frozen

854 in liquid nitrogen and preserved at -80 ºC. DNA contained in particles retained in the 3
855 µm and 0.2 µm filters was extracted by using the PowerSoil DNA isolation kit (MoBio
856 Laboratories Inc., CA, USA) and the PowerWater DNA isolation kit (MoBio
857 Laboratories Inc., CA, USA), respectively, according to the manufacturer's instructions.
858 Prokaryote community composition was assessed by sequencing the V4 and V5 regions
859 of the 16S rRNA gene (16S rDNA) from 0.2 µm Serivex by using the universal primers
860 "515F and 926R" (Parada *et al.*, 2016). Eukaryote community composition from both 3
861 µm and 0.2 µm filters was assessed by sequencing the V4 region from the 18S rRNA
862 gene (18S rDNA) using the primers "TAReuk454FWD1" and "TAReukREV3"
863 (Logares *et al.*, 2014). Amplified regions were sequenced with the Illumina MiSeq
864 platform (paired-end reads; 2 × 300 bp) at the Research and Testing Laboratory
865 (Lubbock, TX, USA) and subsequently analyzed following the DADA2 pipeline
866 (Callahan *et al.*, 2016). The SILVA reference database (Quast *et al.*, 2012) was used for
867 taxonomic assignment of 16S ASVs (amplicon sequence variant). The PR2 (Guillou *et*
868 *al.*, 2013) and the marine protist database from the BioMarks project (Massana *et al.*,
869 2015) were used for the taxonomic assignment of 18S ASVs. The data for this study
870 have been deposited in the European Nucleotide Archive (ENA) at EMBL-EBI
871 (https://www.ebi.ac.uk/ena) under accession numbers PRJEB36188 (16S sequences)
872 and PRJEB36099 (18S sequences).

873 The ASV tables of prokaryotes and eukaryotes were subsampled to the number of reads
874 present in the sample with the lowest number of reads, which was 2080 and 1286, for
875 16S rDNA and 18S rDNA, respectively. Rarefaction curves suggest that these minimum
876 sample sizes were adequate to describe prokaryote and eukaryote communities in our
877 samples (Supporting Information Fig. S3). A total of 1550 unique ASVs of prokaryotes
878 were identified. As many ASVs of eukaryotes were present in both size fractions, we

879 combined datasets derived from the 0.2 and the 3 μm filters for eukaryote community
880 analyses. Reads from each filter size were normalized by the filter DNA yield as
881 explained in Dupont *et al.* (2015) and Hernández-Ruiz *et al.* (2018) obtaining 2293
882 unique 18S ASVs. The sequence abundances of the subsampled ASV tables were
883 transformed using the centered log-ratio (clr) (Fernandes *et al.*, 2014; Gloor *et al.*,
884 2017). Zero values were replaced by the minimum value that was larger than 0 divided
885 by 2.

886

887 **Statistical analyses**

888 Water samples were classified for statistical analyses in three water bodies according to
889 their potential density. The upper mixed layer (UML) was determined as the depth
890 where potential density was 0.1 kg m^{-3} higher than in the surface layer (Fernández-
891 Castro *et al.*, 2014). Eastern North Atlantic Central Water (ENACW) was defined as the
892 depth where potential density (σ-t) was higher than 27 kg m^{-3} (potential temperature
893 about 12 ºC) (Pollard and Pu, 1985; Ríos *et al.*, 1992; Liu and Tanhua, 2019). Samples
894 between the UML and the ENACW layer were classified as sub-surface (SSL).

895 Normal distribution was tested by a Kolmogorov-Smirnov test and variables were log-
896 transformed when it was necessary to obtain normality. Analysis of variance (ANOVA)
897 with Bonferroni's pairwise *post-hoc* tests were used to explore the effect of sampling
898 month, water layer and sampling station on B12, NO_3^- and HPO_4^{2-} concentrations in the
899 transect (stn 3 to 6), and on B12, NO_3^-, HPO_4^{2-} concentrations, phytoplankton and
900 prokaryote biomass and production along the short-term time series at stn 3. To evaluate
901 the spatial variability, the effect of water layer and sampling month and station were

evaluated with samples collected on day 1 of each cruise while temporal variability was evaluated with samples taken at stn 3 from day 1 to day 7.

The environmental (temperature, salinity, inorganic nutrients, dissolved organic carbon, dissolved organic nitrogen, and B12) and biological (size-fractionated phytoplankton biomass and production, and prokaryote biomass and production) data were transformed with the square root function to homogenize values, normalized and a Principal Component Analysis (PCA) were conducted to explore the data. Hierarchical cluster analysis was applied to classify individual samples based on the clr abundances of main microbial taxa using Euclidean distance. The depicted microbial taxa were carefully defined based on their abundance and relevance. The criteria to subdivide a taxonomic level was that the relative abundance of the resulting subgroups (lower taxonomic levels) was higher than 5 % in at least one sample. No subdivisions were made for kingdoms or phyla with low relative abundance (e.g Planctomycetes, Verrucomicrobia, Fungi, Rhizaria). Two-way crossed analysis of similarities (ANOSIM, 999 permutations) were applied to the Euclidean distance matrices of (a) environmental variables, and (b) biological variables to evaluate differences among sampling months and layers. A partial mantel test was used to explore the relationship between the distance matrices built from (a) resource variables, (b) clr abundance of major eukaryote taxa, and (c) clr abundance of major prokaryote taxa. For this analysis, only resource variables (i.e, inorganic nutrients, dissolved organic carbon and nitrogen, and vitamin B12) were considered as the main factors directly impacting microbial growth.

Multiple linear regression analysis was conducted to explore the relationship between resource variables and both prokaryote and phytoplankton production and biomass. The

influence of dissolved nutrients (including NO_3^-, NO_2^-, NH_4^+, SiO_4^{4-}, HPO_4^{2-}, dissolved organic carbon, dissolved organic nitrogen, and B12 concentrations) on the microbial community structure was explored by calculating the Pearson coefficient between normalized nutrients and the clr abundance of the main taxonomic groups.

Species co-occurrence analysis was completed using R studio with the package "co-occur" (Griffith *et al.*, 2016), using the default settings of the package. Co-occurrence patterns among pairs of microbial ASVs based on presence/absence data were assessed with the probabilistic approach of Veech (Veech, 2013) to determine positive, negative and random (i.e. not significant) co-occurrence among species. A co-association network was inferred and visualized for each water body with Cytoscape v3.7.1 (Shannon *et al.*, 2003). To visualize the networks we filtered the infrequent ASVs selecting the top 50 most abundant ASVs at each layer (25 prokaryote ASVs and 25 eukaryote ASVs). Networks were compared against 100 randomized versions generated preserving the degree of nodes and edges applying Erdős–Rényi model by using the Network Randomizer App. Topological parameters were calculated with the Network Analyzer tool implemented in the Cytoscape software and these parameters were compared between random and co-occurrence networks to evaluate the arbitrariness of the community structure along the water column.

Author contribution. Eva Teira designed the experiments and Vanessa Joglar carried them out with contributions of Clara Pérez-Martínez, Benjamin Pontiller, Emilio Fernández and Eva Teira. X. A. Álvarez-Salgado was responsible for measuring inorganic and organic nutrients and Ana Gago and Jose M. Leao for dissolved B12

concentrations. Daniel Lundin, Benjamin Pontiller and Jarone Pinhassi processed the sequencing data. Vanessa Joglar and Eva Teira interpreted the results and prepared the manuscript. All authors contributed to the further development of the manuscript and approved the final version.

Competing interests. The authors declare that they have no conflict of interest.

Acknowledgments. We thank all the people involved in the project ENVISION for helping with sampling and analytical work. We also thank the crew of the Ramón Margalef for their help during the work at sea. From IIM-CSIC, V. Vieitez and M.J. Pazó performed the inorganic and organic nutrient analysis. From Linnaeus University, J. Lautin collaborated with the metagenomic analysis. The scintillation counter was supported by the 2006-06 ICTS project of the Ministry of Science and Innovation at the Spanish Institute of Oceanography. This research was supported by the Spanish Ministry of Economy and Competitiveness through the ENVISION (CTM2014-59031-P) and INTERES (CTM2017-83362-R) projects. Further support was provided by the Swedish Research Council VR. Vanessa Joglar was supported by an FPI fellowship from the Spanish Ministry of Economy and Competitiveness.

970 **References**

971 Álvarez-Salgado, X.A., Figueiras, F.G., Pérez, F.F., Groom, S., Nogueira, E., Borges,
972 A. V., et al. (2003) The Portugal coastal counter current off NW Spain: New
973 insights on its biogeochemical variability. *Prog Oceanogr* **56**: 281–321.

974 Álvarez-Salgado, X.A., Gago, J., Míguez, B.M., Gilcoto, M., and Pérez, F.F. (2000)
975 Surface waters of the NW Iberian margin: Upwelling on the shelf versus
976 outwelling of upwelled waters from the Rías Baixas. *Estuar Coast Shelf Sci* **51**:
977 821–837.

978 Amin, S.A., Hmelo, L.R., Van Tol, H.M., Durham, B.P., Carlson, L.T., Heal, K.R., et
979 al. (2015) Interaction and signalling between a cosmopolitan phytoplankton and
980 associated bacteria. *Nature* **522**: 98–101.

981 Amin, S.A., Parker, M.S., and Armbrust, E. V. (2012) Interactions between Diatoms
982 and Bacteria. *Microbiol Mol Biol Rev* **76**: 667–684.

983 Banerjee, R. (1997) The Yin-Yang of cobalamin biochemistry. *Chem Biol* **4**: 175–186.

984 Banerjee, R. and Ragsdale, S.W. (2003) The Many Faces of Vitamin B_{12} : Catalysis by
985 Cobalamin-Dependent Enzymes. *Annu Rev Biochem* **72**: 209–247.

986 Barber-Lluch, E., Hernández-Ruiz, M., Prieto, A., Fernández, E., and Teira, E. (2019)
987 Role of Vitamin B12 in the microbial plankton response to nutrient enrichment.
988 *Mar Ecol Prog Ser* **626**: 29–42.

989 Barton, E.D., Largier, J.L., Torres, R., Sheridan, M., Trasviña, A., Souza, A., et al.
990 (2015) Coastal upwelling and downwelling forcing of circulation in a semi-
991 enclosed bay: Ria de Vigo. *Prog Oceanogr* **134**: 173–189.

992 Barton, E.D., Torres, R., Figueiras, F.G., Gilcoto, M., and Largier, J. (2016) Journal of

993 Geophysical Research: Oceans. *J Geophys Res Ocean* **121**: 7088–7107.

994 Bertrand, E.M. and Allen, A.E. (2012) Influence of vitamin B auxotrophy on nitrogen
995 metabolism in eukaryotic phytoplankton. *Front Microbiol* **3**: 1–16.

996 Bertrand, E.M., Allen, A.E., Dupont, C.L., Norden-Krichmar, T.M., Bai, J., Valas, R.E.,
997 and Saito, M.A. (2012) Influence of cobalamin scarcity on diatom molecular
998 physiology and identification of a cobalamin acquisition protein. *Proc Natl Acad*
999 *Sci* **109**: E1762–E1771.

1000 Bertrand, E.M., McCrow, J.P., Moustafa, A., Zheng, H., McQuaid, J.B., Delmont, T.O.,
1001 et al. (2015) Phytoplankton-bacterial interactions mediate micronutrient
1002 colimitation at the coastal Antarctic sea ice edge. *Proc Natl Acad Sci U S A* **112**:
1003 9938–9943.

1004 Bertrand, E.M., Moran, D.M., McIlvin, M.R., Hoffman, J.M., Allen, A.E., and Saito,
1005 M.A. (2013) Methionine synthase interreplacement in diatom cultures and
1006 communities: Implications for the persistence of B12 use by eukaryotic
1007 phytoplankton. *Limnol Oceanogr* **58**: 1431–1450.

1008 Bertrand, E.M., Saito, M.A., Lee, P.A., Dunbar, R.B., Sedwick, P.N., and Ditullio, G.R.
1009 (2011) Iron limitation of a springtime bacterial and phytoplankton community in
1010 the Ross Sea: Implications for vitamin B12 nutrition. *Front Microbiol* **2**: 1–12.

1011 Biebl, H., Allgaier, M., Tindall, B.J., Koblizek, M., Lünsdorf, H., Pukall, R., and
1012 Wagner-Döbler, I. (2005) Dinoroseobacter shibae gen. nov., sp. nov., a new
1013 aerobic phototrophic bacterium isolated from dinoflagellates. *Int J Syst Evol*
1014 *Microbiol* **55**: 1089–1096.

1015 Blanton, J.O., Atkinson, L.P., Fernandez de Castillejo, F., and Lavin Montero, A.

(1984) Coastal upwelling off the Rias Bajas, Galicia, Northwest Spain I: Hydrographic studies. *Reun ConsIntExplorMer* **183**: 79–90.

Brown, K.L. (2005) Chemistry and enzymology of vitamin B12. *Chem Rev* **105**: 2075–2149.

Callahan, B.J., McMurdie, P.J., Rosen, M.J., Han, A.W., Johnson, A.J.A., and Holmes, S.P. (2016) DADA2: High-resolution sample inference from Illumina amplicon data. *Nat Methods* **13**: 581–583.

Calvo-Díaz, A. and Morán, X.A.G. (2006) Seasonal dynamics of picoplankton in shelf waters of the southern Bay of Biscay. *Aquat Microb Ecol* **42**: 159–174.

Carlucci, A.F. and Bowes, P.M. (1970) Vitamin production and utilization by phytoplankton in mixed culture. *J Phycol* **6**: 393–400.

Carlucci, A.F. and Cuhel, R.L. (1977) Vitamins in the south polarseas: distribution and significance of dissolved and particulatevitamin B12, thiamine and biotin in the Southern IndianOcean. In, Llano,G. (ed), *Adaptations within marine ecosystems.* Smithsonian Institution, pp. 115–128.

Carlucci, A.F., Silbernagel, S.B., and McNally, P.M. (1969) Influence of temeprature and solar radiation on persistence of vitamin B12, thiamine and biotin in seawater. *J Phycol* **5**: 302–305.

Cermeño, P., Marañón, E., Pérez, V., Serret, P., Fernández, E., and Castro, C.G. (2006) Phytoplankton size structure and primary production in a highly dynamic coastal ecosystem (Ría de Vigo, NW-Spain): Seasonal and short-time scale variability. *Estuar Coast Shelf Sci* **67**: 251–266.

Cirri, E. and Pohnert, G. (2019) Algae−bacteria interactions that balance the planktonic

microbiome. *New Phytol* **223**: 100–106.

Cohen, N.R., A. Ellis, K., Burns, W.G., Lampe, R.H., Schuback, N., Johnson, Z., et al. (2017) Iron and vitamin interactions in marine diatom isolates and natural assemblages of the Northeast Pacific Ocean. *Limnol Oceanogr* **62**: 2076–2096.

Cooper, M.B., Kazamia, E., Helliwell, K.E., Kudahl, U.J., Sayer, A., Wheeler, G.L., and Smith, A.G. (2019) Cross-exchange of B-vitamins underpins a mutualistic interaction between Ostreococcus tauri and Dinoroseobacter shibae. *ISME J* **13**: 334–345.

Cooper, M.B. and Smith, A.G. (2015) Exploring mutualistic interactions between microalgae and bacteria in the omics age. *Curr Opin Plant Biol* **26**: 147–153.

Croft, M.T., Lawrence, A.D., Raux-Deery, E., Warren, M.J., and Smith, A.G. (2005) Algae acquire vitamin B12 through a symbiotic relationship with bacteria. *Nature* **438**: 90–93.

Croft, M.T., Warren, M.J., and Smith, A.G. (2006) Algae need their vitamins. *Eukaryot Cell* **5**: 1175–1183.

Doxey, A.C., Kurtz, D.A., Lynch, M.D.J., Sauder, L.A., and Neufeld, J.D. (2015) Aquatic metagenomes implicate Thaumarchaeota in global cobalamin production. *ISME J* **9**: 461–471.

Droop, M.R. (1957) Vitamin B12 in marine ecology [2]. *Nature* **180**: 1041–1042.

Dupont, C.L., Mccrow, J.P., Valas, R., Moustafa, A., Walworth, N., Goodenough, U., et al. (2015) Genomes and gene expression across light and productivity gradients in eastern subtropical Pacific microbial communities. *ISME J* **9**: 1076–1092.

Durham, B.P., Sharma, S., Luo, H., Smith, C.B., Amin, S.A., Bender, S.J., et al. (2015)

Cryptic carbon and sulfur cycling between surface ocean plankton. *Proc Natl Acad Sci U S A* **112**: 453–457.

Elias, M., Gompert, Z., Jiggins, C., and Willmott, K. (2008) Mutualistic interactions drive ecological niche convergence in a diverse butterfly community. *PLoS Biol* **6**: 2642–2649.

Ellis, K.A., Cohen, N.R., Moreno, C., and Marchetti, A. (2017) Cobalamin-independent Methionine Synthase Distribution and Influence on Vitamin B12 Growth Requirements in Marine Diatoms. *Protist* **168**: 32–47.

Elser, J.J., Stabler, L.B., and Hassett, R.P. (1995) Nutrient limitation of bacterial growth rates in lakes and oceans: a comparative study. *Aquat Microb Ecol* **9**: 105–110.

Fernandes, A.D., Reid, J.N., Macklaim, J.M., McMurrough, T.A., Edgell, D.R., and Gloor, G.B. (2014) Unifying the analysis of high-throughput sequencing datasets: characterizing RNA-seq, 16S rRNA gene sequencing and selective growth experiments by compositional data analysis. *Microbiome* **2**: 15.

Fernández-Castro, B., Mouriño-Carballido, B., Benítez-Barrios, V.M., Chouciño, P., Fraile-Nuez, E., Graña, R., et al. (2014) Microstructure turbulence and diffusivity parameterization in the tropical and subtropical Atlantic, Pacific and Indian Oceans during the Malaspina 2010 expedition. *Deep Res Part I Oceanogr Res Pap* **94**: 15–30.

Fietz, S., Martínez-Garcia, A., Rueda, G., Peck, V.L., Huguet, C., Escala, M., and Rosell-Melé, A. (2011) Crenarchaea and phytoplankton coupling in sedimentary archives: Common trigger or metabolic dependence? *Limnol Oceanogr* **56**: 1907–1916.

1085 Figueiras, F.G., Abarta, U., and Fernández Reiriz, M.J. (2002) Coastal upwelling,
1086 primary production and mussel growth in the Rías Baixas of Galicia.
1087 *Hydrobiologia* **484**: 121–131.

1088 Fisher, T.R., Peele, E.R., Ammerman, J.W., and Jr, L.W.H. (1992) Nutrient limitation
1089 of phytoplankton in Chesapeake Bay. *Mar Ecol Prog Ser* **82**: 51–63.

1090 Fraga, F. (1981) Upwelling off the Galacian Coast, northwest Spain. In, Richards,F.A.
1091 (ed), *Coastal and Estuarine Sciences*., pp. 176–182.

1092 Gasol, J.M. and Del Giorgio, P.A. (2000) Using flow cytometry for counting natural
1093 planktonic bacteria and understanding the structure of planktonic bacterial
1094 communities. *Sci Mar* **64**: 197–224.

1095 Gloor, G.B., Macklaim, J.M., Pawlowsky-Glahn, V., and Egozcue, J.J. (2017)
1096 Microbiome datasets are compositional: And this is not optional. *Front Microbiol*
1097 **8**: 1–6.

1098 Gobler, C.J., Norman, C., Panzeca, C., Taylor, G.T., and Sañudo-Wilhelmy, S.A.
1099 (2007) Effect of B-vitamins (B1, B12) and inorganic nutrients on algal bloom
1100 dynamics in a coastal ecosystem. *Aquat Microb Ecol* **49**: 181–194.

1101 Gómez-Gesteira, M., de Castro, M., Prego, R., and P□rez-Villar, V. (2001) An unusual
1102 two layered tidal circulation induced by stratification and wind in the Ría of
1103 Pontevedra (NW Spain). *Estuar Coast Shelf Sci* **52**: 555–563.

1104 Gong, W., Browne, J., Hall, N., Schruth, D., Paerl, H., and Marchetti, A. (2017)
1105 Molecular insights into a dinoflagellate bloom. *ISME J* **11**: 439–452.

1106 Gonzalez-Nuevo, G., Gago, J., and Cabanas, J.M. (2014) Upwelling index: A powerful
1107 tool for marine research in the NW Iberian upwelling system. *J Oper Oceanogr* **7**:

47–57.

Grant, M.A., Kazamia, E., Cicuta, P., and Smith, A.G. (2014) Direct exchange of vitamin B12 is demonstrated by modelling the growth dynamics of algal–bacterial cocultures. *ISME J* **8**: 1418–1427.

Griffith, D.M., Veech, J.A., and Marsh, C.J. (2016) Cooccur: Probabilistic species co-occurrence analysis in R. *J Stat Softw* **69**: 1–17.

Guillou, L., Bachar, D., Audic, S., Bass, D., Berney, C., Bittner, L., et al. (2013) The Protist Ribosomal Reference database (PR2): a catalog of unicellular eukaryote Small Sub-Unit rRNA sequences with curated taxonomy. *Nucleic Acids Res* **41**: D597–D604.

Haines, K.C. and Guillard, R.R.L. (1974) Growth of vitamin B12-requiring marine diatoms in mixed laboratory cultures with vitamin B12-producing marine bacteria. *J Phycol* **10**: 245–252.

Heal, K.R., Carlson, L.T. ruxa., Devol, A.H., Armbrust, E.V., Moffett, J.W., Stahl, D.A., and Ingalls, A.E. (2014) Determination of four forms of vitamin B12 and other B vitamins in seawater by liquid chromatography/tandem mass spectrometry. *Rapid Commun Mass Spectrom* **28**: 2398–2404.

Heal, K.R., Qin, W., Ribalet, F., Bertagnolli, A.D., Coyote-Maestas, W., Hmelo, L.R., et al. (2017) Two distinct pools of B12 analogs reveal community interdependencies in the ocean. *Proc Natl Acad Sci U S A* **114**: 364–369.

Helliwell, K.E. (2017) The roles of B vitamins in phytoplankton nutrition: New perspectives and prospects. *New Phytol*.

Helliwell, K.E., Lawrence, A.D., Holzer, A., Kudahl, U.J., Sasso, S., Kräutler, B., et al.

(2016) Cyanobacteria and Eukaryotic Algae Use Different Chemical Variants of Vitamin B12. *Curr Biol* **26**: 999–1008.

Helliwell, K.E., Scaife, M.A., Sasso, S., Paula, A., Araujo, U., Purton, S., and Smith, A.G. (2014) Unraveling vitamin B12-responsive gene regulation in algae. *Plant Physiol* **165**: 388–397.

Helliwell, K.E., Wheeler, G.L., Leptos, K.C., Goldstein, R.E., and Smith, A.G. (2011) Insights into the evolution of vitamin B 12 auxotrophy from sequenced algal genomes. *Mol Biol Evol* **28**: 2921–2933.

Hernández-Ruiz, M., Barber-Lluch, E., Prieto, A., Álvarez-Salgado, X.A., Logares, R., and Teira, E. (2018) Seasonal succession of small planktonic eukaryotes inhabiting surface waters of a coastal upwelling system. *Environ Microbiol* **20**: 2955–2973.

Joglar, V., Prieto, A., Barber-Lluch, E., Hernández-Ruiz, M., Fernández, E., and Teira, E. (2020) Spatial and temporal variability in the response of phytoplankton and prokaryotes to B-vitamin amendments in an upwelling system. *Biogeosciences* **17**: 2807–2823.

Joint, I., Hendrikson, P., Fonnes, G.A., Bourne, D., Thingstad, T.F., and Rieman, B. (2002) Competition for inorganic nutrients between phytoplankton and bacterioplancton in nutriend manipulated mesocosms. *Aquat Microb Ecol* **29**: 145–159.

Juzeniene, A., Baturaite, Z., Lagunova, Z., Grigalavicius, M., Porojnicu, A.C., Bruland, Ø.S., and Moan, J. (2015) Influence of multiple UV exposures on serum cobalamin and vitamin D levels in healthy females. *Scand J Public Health* **43**: 324–330.

Juzeniene, A. and Nizauskaite, Z. (2013) Photodegradation of cobalamins in aqueous

1154 solutions and in human blood. *J Photochem Photobiol B Biol* **122**: 7–14.

1155 Karl, D.M. (2002) Nutrient dynamics in the deep blue sea. *Trends Microbiol* **10**: 410–
1156 418.

1157 Kazamia, E., Czesnick, H., Nguyen, T.T. Van, Croft, M.T., Sherwood, E., Sasso, S., et
1158 al. (2012) Mutualistic interactions between vitamin B12-dependent algae and
1159 heterotrophic bacteria exhibit regulation. *Environ Microbiol* **14**: 1466–1476.

1160 Koch, F., Hattenrath-Lehmann, T.K., Goleski, J.A., Sañudo-Wilhelmy, S., Fisher, N.S.,
1161 and Gobler, C.J. (2012) Vitamin B1 and B12 uptake and cycling by plankton
1162 communities in coastal ecosystems. *Front Microbiol* **3**: 1–11.

1163 Koch, F., Marcoval, M.A., Panzeca, C., Bruland, K.W., Sañudo-Wilhelmy, S.A., and
1164 Gobler, C.J. (2011) The effect of vitamin B12 on phytoplankton growth and
1165 community structure in the Gulf of Alaska. *Limnol Oceanogr* **56**: 1023–1034.

1166 Koutmos, M., Datta, S., Pattridge, K.A., Smith, J.L., and Matthews, R.G. (2009)
1167 Insights into the reactivation of cobalamin-dependent methionine synthase. *Proc*
1168 *Natl Acad Sci U S A* **106**: 18527–32.

1169 Liu, M. and Tanhua, T. (2019) Distribution of Water Masses in the Atlantic Ocean
1170 based on GLODAPv2. *Ocean Sci Discuss* 1–32.

1171 Logares, R., Sunagawa, S., Salazar, G., Cornejo-Castillo, F.M., Ferrera, I., Sarmento,
1172 H., et al. (2014) Metagenomic 16S rDNA Illumina tags are a powerful alternative
1173 to amplicon sequencing to explore diversity and structure of microbial
1174 communities. *Environ Microbiol* **16**: 2659–2671.

1175 Lovdal, T., Eichner, C., Grossart, H.P., Carbonnel, V., Chou, L., Martin-Jezequel, V.,
1176 and Thingstad, T.F. (2008) Competition for inorganic and organic forms of

1177 nitrogen and phosphorous between phytoplankton and bacteria during an Emiliania
1178 huxleyi spring bloom. *Biogeosciences* **5**: 371–383.

1179 Madigan, M.T., Martinko, J., and Parker, J. (2005) Brock Biology of Micro-Organisms,
1180 11th ed. Pearson (ed) Boston: Prentice Hall.

1181 Marañón, E., Holligan, P., Barciela, R., González, N., Mouriño, B., Pazó, M., and
1182 Varela, M. (2001) Patterns of phytoplankton size structure and productivity in
1183 contrasting open-ocean environments. *Mar Ecol Prog Ser* **216**: 43–56.

1184 Marsh, E.N. (1999) Coenzyme B12 (cobalamin)-dependent enzymes. *Essays Biochem*
1185 **34**: 139–54.

1186 Martens, J.H., Barg, H., Warren, M., and Jahn, D. (2002) Microbial production of
1187 vitamin B12. *Appl Microbiol Biotechnol* **58**: 275–285.

1188 Martínez-García, S., Fernández, E., Calvo-Díaz, A., Marañón, E., Morán, X.A.G., and
1189 Teira, E. (2010) Response of heterotrophic and autotrophic microbial plankton to
1190 inorganic and organic inputs along a latitudinal transect in the Atlantic Ocean.
1191 *Biogeosciences* **7**: 1701–1713.

1192 Massana, R., Gobet, A., Audic, S., Bass, D., Bittner, L., Boutte, C., et al. (2015) Marine
1193 protist diversity in European coastal waters and sediments as revealed by high-
1194 throughput sequencing. *Environ Microbiol* **17**: 4035–4049.

1195 Matthews, R.G., Smith, A.E., Zhou, Z.S., Taurog, R.E., Bandarian, V., Evans, J.C., and
1196 Ludwig, M. (2003) Cobalamin-dependent and cobalamin-independent methionine
1197 synthases: Are there two solutions to the same chemical problem? *Helv Chim Acta*
1198 **86**: 3939–3954.

1199 Menzel, D.W. and Spaeth, J.P. (1962) Occurrence of vitamin B_{12} in the Sargasso Sea.

1200 *Limnol Oceanogr* **7**: 151–154.

1201 Monteverde, D.R., Gómez-Consarnau, L., Suffridge, C., and Sañudo-Wilhelmy, S.A.
1202 (2017) Life's utilization of B vitamins on early Earth. *Geobiology* **15**: 3–18.

1203 Moustafa, A., Evans, A.N., Kulis, D.M., Hackett, J.D., Erdner, D.L., Anderson, D.M.,
1204 and Bhattacharya, D. (2010) Transcriptome profiling of a toxic dinoflagellate
1205 reveals a gene-rich protist and a potential impact on gene expression due to
1206 bacterial presence. *PLoS One* **5**:.

1207 Okbamichael, M. and Sañudo-Wilhelmy, S.A. (2004) A new method for the
1208 determination of Vitamin B12 in seawater. *Anal Chim Acta* **517**: 33–38.

1209 Paerl, R.W., Bertrand, E.M., Allen, A.E., Palenik, B., and Azam, F. (2015) Vitamin B1
1210 ecophysiology of marine picoeukaryotic algae: Strain-specific differences and a
1211 new role for bacteria in vitamin cycling. *Limnol Oceanogr* **60**: 215–228.

1212 Paerl, R.W., Sundh, J., Tan, D., Svenningsen, S.L., Hylander, S., Pinhassi, J., et al.
1213 (2018) Prevalent reliance of bacterioplankton on exogenous vitamin B1 and
1214 precursor availability. *Proc Natl Acad Sci U S A* **115**: E10447–E10456.

1215 Palenik, B., Grimwood, J., Aerts, A., Rouzé, P., Salamov, A., Putnam, N., et al. (2007)
1216 The tiny eukaryote Ostreococcus provides genomic insights into the paradox of
1217 plankton speciation. *Proc Natl Acad Sci U S A* **104**: 7705–7710.

1218 Panzeca, C., Beck, A.J., Tovar-Sanchez, A., Segovia-Zavala, J., Taylor, G.T., Gobler,
1219 C.J., and Sañudo-Wilhelmy, S.A. (2009) Distributions of dissolved vitamin B12
1220 and Co in coastal and open-ocean environments. *Estuar Coast Shelf Sci* **85**: 223–
1221 230.

1222 Parada, A.E., Needham, D.M., and Fuhrman, J.A. (2016) Every base matters: Assessing

small subunit rRNA primers for marine microbiomes with mock communities, time series and global field samples. *Environ Microbiol* **18**: 1403–1414.

Piedracoba, S., Álvarez-Salgado, X.A., Rosón, G., and Herrera, J.L. (2005) Short-timescale thermohaline variability and residual circulation in the central segment of the coastal upwelling system of the Ría de Vigo (northwest Spain) during four contrasting periods. *J Geophys Res C Ocean* **110**: 1–15.

Piehler, M.F., Twomey, L.J., Hall, N.S., and Paerl, H.W. (2004) Impacts of inorganic nutrient enrichment on phytoplankton community structure and function in Pamlico Sound, NC, USA. *Estuar Coast Shelf Sci* **61**: 197–209.

Pollard, R.T. and Pu, S. (1985) Structure and circulation of the Upper Atlantic Ocean northeast of the Azores. *Prog Oceanogr* **14**: 443–462.

Provasoli, L. (1963) Organic regulation of phytoplankton fertility. *sea* **2**: 165–219.

Quast, C., Pruesse, E., Yilmaz, P., Gerken, J., Schweer, T., Yarza, P., et al. (2012) The SILVA ribosomal RNA gene database project: improved data processing and web-based tools. *Nucleic Acids Res* **41**: D590–D596.

Ríos, A.F., Pérez, F.F., and Fraga, F. (1992) Water masses in the upper and middle North Atlantic Ocean east of the Azores. *Deep Sea Res Part A Oceanogr Res Pap* **39**: 645–658.

Rodionov, D.A., Vitreschak, A.G., Mironov, A.A., and Gelfand, M.S. (2003) Comparative Genomics of the Vitamin B12 Metabolism and Regulation in Prokaryotes. *J Biol Chem* **278**: 41148–41159.

Roth, J., Lawrence, J., and Bobik, T. (1996) Cobalamin (coenzyme B12): synthesis and biological significance. *Annu Rev Microbiol* **50**: 137–181.

1246 Sañudo-Wilhelmy, S.A., Cutter, L.S., Durazo, R., Smail, E.A., Gómez-Consarnau, L.,
1247 Webb, E.A., et al. (2012) Multiple B-vitamin depletion in large areas of the coastal
1248 areas. *Proc Natl Acad Sci U S A* **109**: 14041–14045.

1249 Sañudo-Wilhelmy, S.A., Gobler, C.J., Okbamichael, M., and Taylor, G.T. (2006)
1250 Regulation of phytoplankton dynamics by vitamin B12. *Geophys Res Lett* **33**: 10–
1251 13.

1252 Sañudo-Wilhelmy, S.A., Gómez-Consarnau, L., Suffridge, C., and Webb, E.A. (2014)
1253 The role of B vitamins in marine biogeochemistry. *Ann Rev Mar Sci* **6**: 339–367.

1254 Seymour, J.R., Amin, S.A., Raina, J.B., and Stocker, R. (2017) Zooming in on the
1255 phycosphere: The ecological interface for phytoplankton-bacteria relationships.
1256 *Nat Microbiol* **2**:.

1257 Shannon, P., Markiel, A., Ozier, O., Baliga, N.S., Wang, J.T., Ramage, D., et al. (2003)
1258 Cytoscape: A software environment for integrated models of biomolecular
1259 interaction networks. *Genome Res* **13**: 2498–2504.

1260 Smith, D.C. and Azam, F. (1992) A simple, economical method for measuring bacterial
1261 protein synthesis rates in seawater using 3H-leucine1. *Mar Microb Food Webs* **6**:
1262 107–114.

1263 Stupperich, E. and Krautler, B. (1988) Pseudo vitamin B12 or 5-ydroxybenzimidazolyl-
1264 cobamide are the corrinoids found in methanogenic bacteria. *Arch Microbiol* **149**:
1265 268–271.

1266 Suffridge, C., Cutter, L., and Sañudo-Wilhelmy, S.A. (2017) A new analytical method
1267 for direct measurement of particulate and dissolved B-vitamins and their congeners
1268 in seawater. *Front Mar Sci* **4**: 1–11.

1269 Suffridge, C.P., Gómez-Consarnau, L., Monteverde, D.R., Cutter, L., Arístegui, J.,
1270 Alvarez-Salgado, X.A., et al. (2018) B Vitamins and Their Congeners as Potential
1271 Drivers of Microbial Community Composition in an Oligotrophic Marine
1272 Ecosystem. *J Geophys Res Biogeosciences* **123**: 2890–2907.

1273 Swift, D.G. (1981) Vitamin levels in the Gulf of Maine and ecological significance of
1274 vitamin B12 there. *J Mar Res* **39**: 375–403.

1275 Swift, D.G. (1980) Vitamins and phytoplankton growth. *Physiol Ecol Phytoplankt* 329–
1276 368.

1277 Tang, Y., Koch, F., and Gobler, C.J. (2010) Most harmful algal bloom species are
1278 vitamin B1 and B12 auxotrophs. *Proc Natl Acad Sci* **107**: 20756–20761.

1279 Taylor, G.T. and Sullivan, C.W. (2008) Vitamin B12 and cobalt cycling among diatoms
1280 and bacteria in Antarctic sea ice microbial communities. *Limnol Oceanogr* **53**:
1281 1862–1877.

1282 Teira, E., Aranguren-Gassis, M., González, J., Martínez-García, S., Pérez, P., and
1283 Serret, P. (2009) Influence of allochthonous matter on microbial community
1284 structure and function in an upwelling system off the northwest Iberian Peninsula.
1285 *Aquat Microb Ecol* **55**: 81–93.

1286 Vaid, F.H.M., Zahid, S., Faiyaz, A., Qadeer, K., Gul, W., Anwar, Z., and Ahmad, I.
1287 (2018) Photolysis of methylcobalamin in aqueous solution: A kinetic study. *J*
1288 *Photochem Photobiol A Chem* **362**: 40–48.

1289 Veech, J.A. (2013) A probabilistic model for analysing species co-occurrence. *Glob*
1290 *Ecol Biogeogr* **22**: 252–260.

1291 Villegas-Mendoza, J., Cajal-Medrano, R., and Maske, H. (2019) B12 production by

1292 marine microbial communities and Dinoroseobacter shibae continuous cultures
1293 under different growth and respiration rates. *Aquat Microb Ecol* **83**: 251–262.

1294 Wagner-Döbler, I., Ballhausen, B., Berger, M., Brinkhoff, T., Buchholz, I., Bunk, B., et
1295 al. (2010) The complete genome sequence of the algal symbiont Dinoroseobacter
1296 shibae: A hitchhiker's guide to life in the sea. *ISME J* **4**: 61–77.

1297 Warren, M.J., Raux, E., Schubert, H.L., and Escalante-Semerena, J.C. (2002) The
1298 biosynthesis of adenosylcobalamin (vitamin B12). *Nat Prod Rep* **19**: 390–412.

1299 Watanabe, F., Katsura, H., Takenaka, S., Fujita, T., Abe, K., Tamura, Y., et al. (1999)
1300 Pseudovitamin B12 is the predominant cobamide of an algal health food, spirulina
1301 tablets. *J Agric Food Chem* **47**: 4736–4741.

1302 Wooster, W.S., Bakun, A., and McLain, D.R. (1976) Seasonal upwelling cycle along
1303 the eastern boundary of the north Atlantic. *J Mar Res* **34**: 131–141.

1304

Tables and Figures

Table 1: Multiple linear regression models for the variables listed in the first column, showing the Beta coefficients for the different explanatory variables in rows. The last column (resource variables) shows the R2 adjusted of the models excluding biotic variables (i.e. PB, HPP, PP, and Chl-*a*). B12: vitamin B12 (CB12+HB12), NO_3^-: nitrate, NO_2^-: nitrite, NH_4^+: ammonium, HPO_4^{2-}: phosphate, SiO_4^{4-}: silicate, DOC: dissolved organic carbon, DON: dissolved organic nitrogen, Chl-a < 3 μm: picophytoplankton biomass, Chl-*a* > 3 μm: nano-microplankton biomass, Chl-*a*: total phytoplankton biomass, PP < 3 μm: picophytoplankton production, PP > 3 μm: nano-microphytoplankton production, PP: total primary production, PB: prokaryote biomass, HPP: heterotrophic prokaryote production. X: variable not entered to create the model, ni: variable not included by the model.

Table 2: Topology of the co-occurrence networks in the upper mixed layer (UML), subsurface layer (SSL) and Eastern North Atlantic Central Water (ENACW). CL, clustering coefficient; CPL, characteristic path length; CL:CLr and CPL:CPLr ratios between de CL or CPL of the real network and the mean CL or CPL of 100 random networks of the same size (indicated with r).

Figure 1: (A) The NW Iberian margin (arrow) and locations of the stations that were sampled highlighting the biological stations (stars). Temporal variability was studied in stn 3 (red). (B) Daily coastal upwelling index (UI) and (C) daily precipitations during each sampling period. Vertical red line shows when cross-shelf transect was sampled.

1329 **Figure 2:** Vertical distribution in the cross-shelf section from stn 3 to stn 6 of
1330 temperature (ºC) showing water layer limits with dotted lines in (A) February, (G) April
1331 and (M) August. The upper mixed layer (UML) and the subsurface layer (SSL) is
1332 separated by the mixed layer deep (MLD) and the Eastern North Atlantic Central Water
1333 (ENACW) is located below the thick dashed line (σ-t, 27 kg m^{-3}). The thick dashed line
1334 (potential density 27 kg m^{-3}) separates the SSL from ENACW since the upper limit of
1335 ENACW is defined as the depth where the potential density (σ-t) is greater than 27 kg
1336 m^{-3} (potential temperature about 12 ºC). Salinity (PSU) in (B) February, (H) April and
1337 (N) August; chlorophyll *a* (Chl-*a*) (mg m^{-3}) in February (C), April (I) and August (O);
1338 dissolved inorganic nitrogen (DIN) (μM) in February (D), April (J) and August (P);
1339 phosphate (HPO_4^{2-}) (μM) in February (E), April (K) and August (Q); and vitamin B12
1340 (pM) in February (F), April (L) and August (R) are also shown.
1341
1342 **Figure 3:** Time course of vertical distribution of physicochemical variables at stn 3 over
1343 the 7-day sampling period. Water layer limits are shown with dotted lines in the
1344 temperature (ºC) plots in (A) February, (L) April and (Q) August. Upper mixed layer
1345 (UML) and subsurface layer (SSL) are separated by mixed layer deep (MLD) and the
1346 Eastern North Atlantic Central Water (ENACW) shown below the thick dashed line (σ-
1347 t, 27 kg m^{-3}). Temporal sections of salinity (PSU) in (B) February, (J) April and (R)
1348 August; chlorophyll *a* (Chl-*a*) (mg m^{-3}) in (C) February, (K) April and (S) August;
1349 dissolved inorganic nitrogen (DIN) (μM) in (D) February, (L) April and (T) August;
1350 dissolved organic nitrogen (DON) (μM) in (E) February, (M) April and (U) August;
1351 phosphate (HPO_4^{2-}) (μM) in (F) February, (N) April and (V) August; dissolved organic
1352 carbon (DOC) (μM) in (G) February, (O) April and (W) August; and B12 (pM) in (H)
1353 February, (P) April and (X) August are also shown.

1354

1355 **Figure 4:** (A) Principal component analysis (PCA) of the abiotic factors measured at stn
1356 3: temperature (T), salinity (Sal), nitrate (NO_3^-), phosphate (HPO_4^{2-}), silicate (SiO_4^{4-}),
1357 dissolved vitamin B12 (B12), nitrite (NO_2^-), ammonium (NH_4^+), dissolved organic
1358 nitrogen (DON) and dissolved organic carbon (DOC). (B) PCA of biological variables
1359 measured at stn 3: picophytoplankton biomass (Chl-*a* < 3 μm), nano-
1360 microphytoplankton biomass (Chl-*a* > 3 μm), picophytoplankton production (PP < 3
1361 μm), nano-microphytoplankton production (PP > 3 μm), prokaryote biomass (PB) and
1362 heterotrophic prokaryote production (HPP). Different symbols stand for different water
1363 layers: upper mixed layer (UML), subsurface layer (SSL), and the Eastern North
1364 Atlantic Central Water (ENACW). Different colors represent different sampling
1365 months: February (green), April (blue) and August (pink).

1366

1367 **Figure 5:** Time course of the vertical distribution of the biological variables at stn 3
1368 over the 7-day sampling period. (A) picophytoplankton biomass (Chl-*a* < 3 μm), (B)
1369 nano-microphytoplankton biomass (Chl-*a* > 3 μm), (C) primary production of
1370 picophytoplankton (PP < 3 μm), (D) primary production of nano-microphytoplankton
1371 (PP > 3 μm), (E) prokaryote biomass (PB) and (F) heterotrophic prokaryote production
1372 (HPP).

1373

1374 **Figure 6:** Time course of the relative abundance of the main taxonomic groups of
1375 prokaryotes and eukaryotes at stn 3 over the 7-day sampling period. Different symbols
1376 stand for different water layers: the upper mixed layer (UML), subsurface layer (SSL)
1377 and the Eastern North Atlantic Central Water (ENACW). Different colors represent
1378 different sampling months: February (green), April (blue) and August (pink) showing

1379 the sampling day. The dendrogram represents the hierarchical clustering of individual
1380 samples based on the clr abundances of major microbial taxa using Euclidean distance.
1381
1382 **Figure 7**: Pearson correlation between the clr-abundance of the main taxonomic groups
1383 and resource variables: nitrate (NO_3^-), dissolved inorganic nitrogen (DIN), phosphate
1384 (HPO_4^{2-}), silicate (SiO_4^{4-}), total dissolved nitrogen (TDN), dissolved vitamin B12
1385 (B12), nitrite (NO_2^-), ammonium (NH_4^+), dissolved organic nitrogen (DON) and
1386 dissolved organic carbon (DOC). The dendrogram represents the hierarchical clustering
1387 of taxonomic groups based on their correlations with abiotic factors (Euclidean
1388 distances). Asterisks indicate statistically significant Pearson correlations.
1389
1390 **Figure 8:** Co-occurrence networks of the 50 most abundant and frequent prokaryote
1391 (diamonds: Archaea, circles: Bacteria) and eukaryote ASVs (hexagons). (A) Upper
1392 mixed layer (UML), (B) subsurface layer and (SSL) (C) Eastern North Atlantic Central
1393 Water (ENACW). Red and blue edges represent positive and negative associations,
1394 respectively. The width of the edges is proportional to the significance level of positive
1395 (coexistence) or negative (mutual exclusion) co-occurrence patterns.

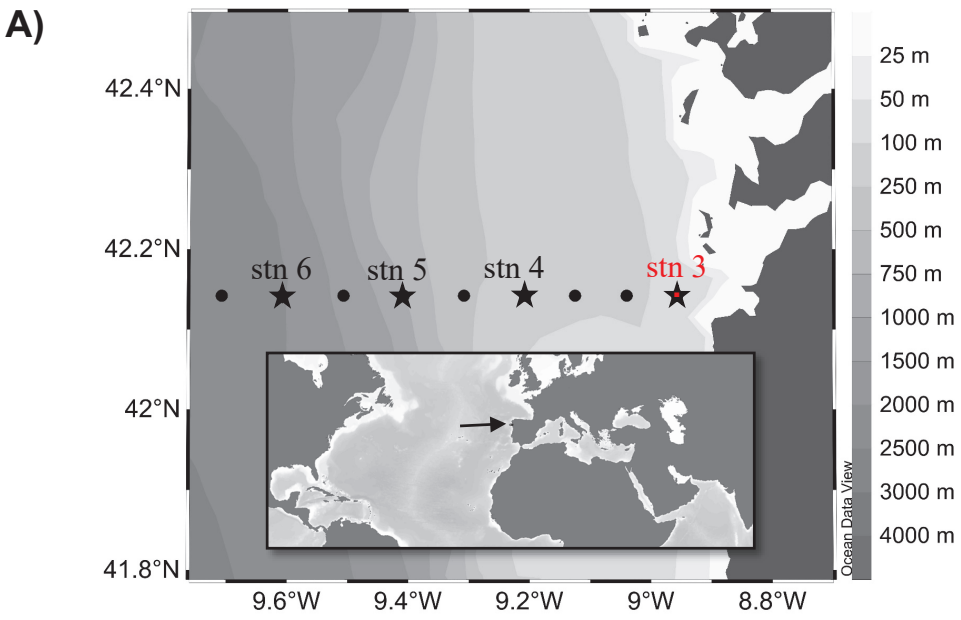
A)
42.4°N
42.2°N
42°N
41.8°N
9.6°W
9.4°W
9.2°W
9°W
8.8°W
stn 6
stn 5
stn 4
stn 3
25 m
50 m
100 m
250 m
500 m
750 m
1000 m
1500 m
2000 m
2500 m
3000 m
4000 m
Ocean Data View

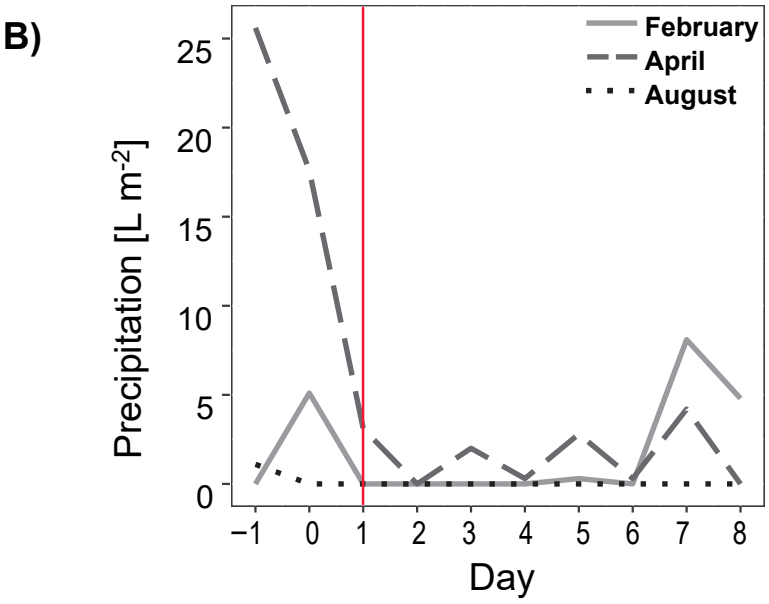
B)
February
April
August
Precipitation [L m-2]
25
20
15
10
5
0
−1
0
1
2
3
4
5
6
7
8
Day

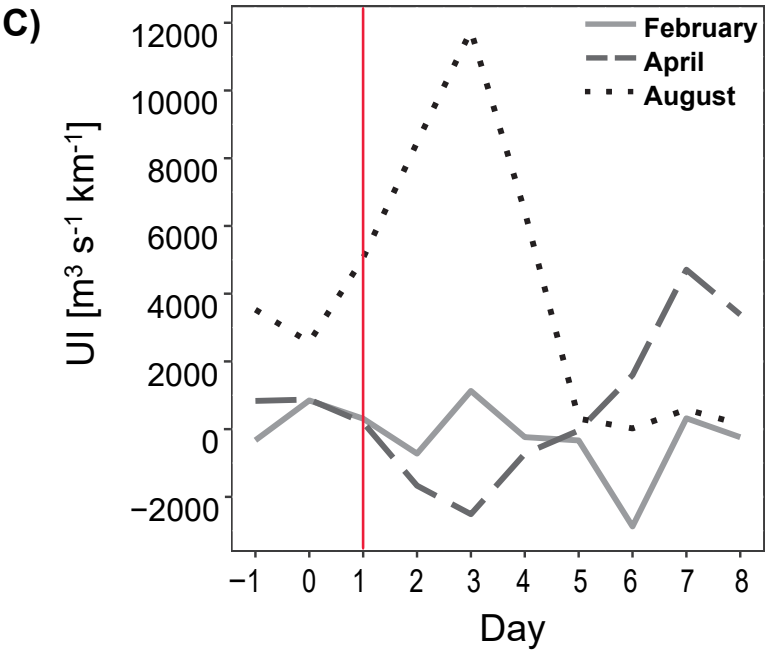
C)
February
April
August
UI [m3 s-1 km-1]
12000
10000
8000
6000
4000
2000
0
−2000
−1
0
1
2
3
4
5
6
7
8
Day

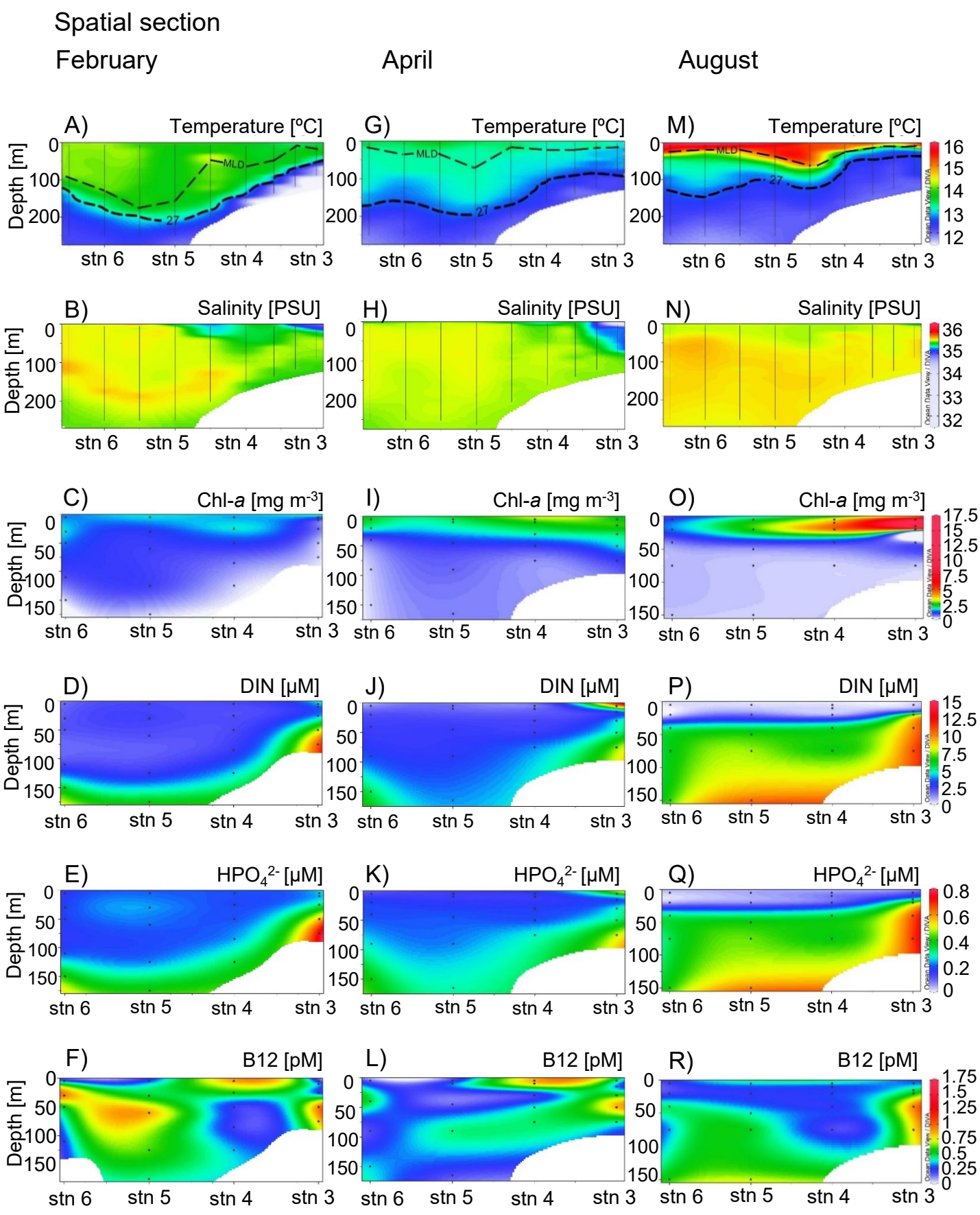
Spatial section
February
April
August
A)
Temperature [ºC]
G)
Temperature [ºC]
M)
Temperature [ºC]
B)
Salinity [PSU]
H)
Salinity [PSU]
N)
Salinity [PSU]
C)
Chl-a [mg m-3]
I)
Chl-a [mg m-3]
O)
Chl-a [mg m-3]
D)
DIN [µM]
J)
DIN [µM]
P)
DIN [µM]
E)
HPO4 2- [µM]
K)
HPO4 2- [µM]
Q)
HPO4 2- [µM]
F)
B12 [pM]
L)
B12 [pM]
R)
B12 [pM]
Depth [m]
MLD
27
stn 6
stn 5
stn 4
stn 3

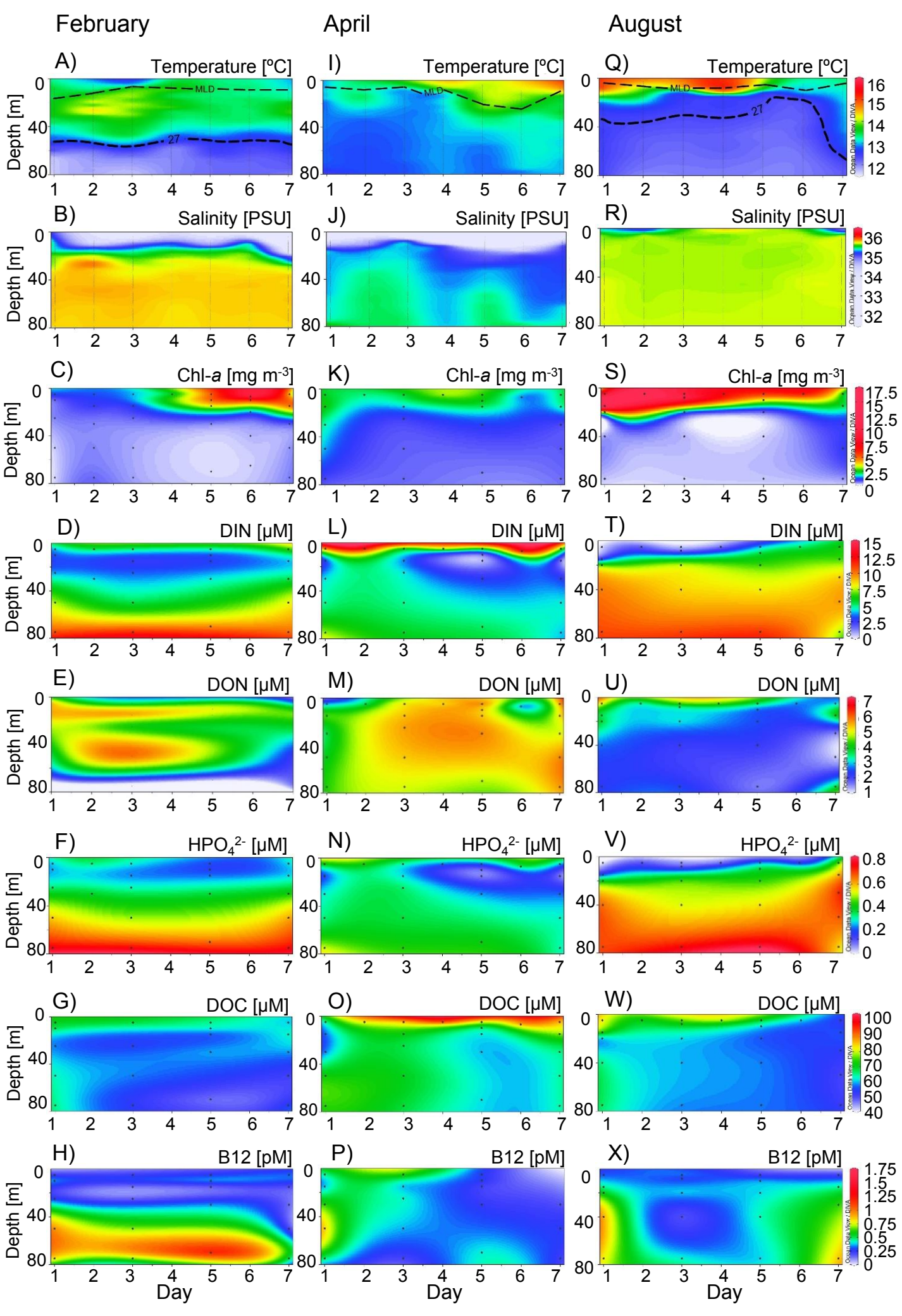
February
April
August
A)
Temperature [ºC]
I)
Temperature [ºC]
Q)
Temperature [ºC]
MLD
27
B)
Salinity [PSU]
J)
Salinity [PSU]
R)
Salinity [PSU]
C)
Chl-a [mg m-3]
K)
Chl-a [mg m-3]
S)
Chl-a [mg m-3]
D)
DIN [µM]
L)
DIN [µM]
T)
DIN [µM]
E)
DON [µM]
M)
DON [µM]
U)
DON [µM]
F)
HPO4 2- [µM]
N)
HPO4 2- [µM]
V)
HPO4 2- [µM]
G)
DOC [µM]
O)
DOC [µM]
W)
DOC [µM]
H)
B12 [pM]
P)
B12 [pM]
X)
B12 [pM]
Depth [m]
Day
Ocean Data View / DIVA

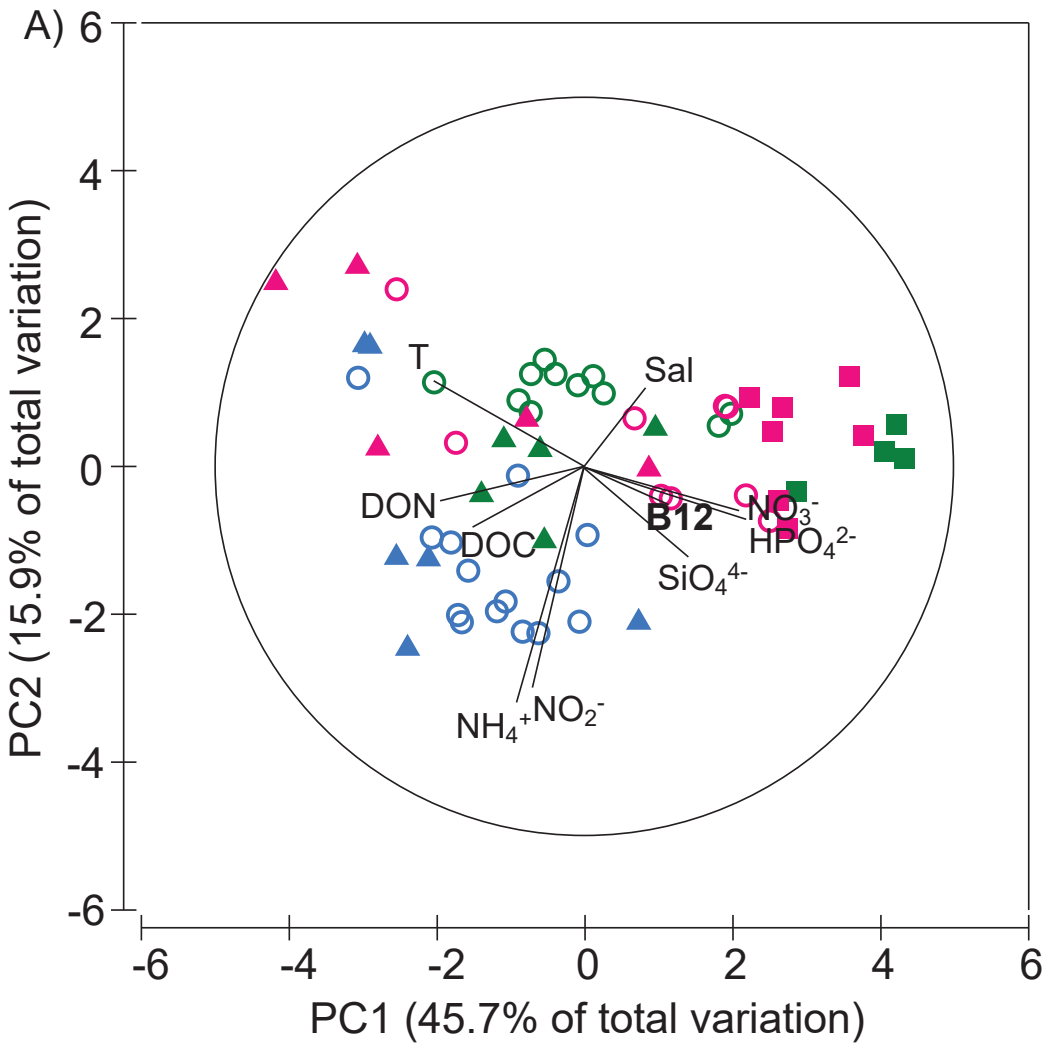
A)
PC2 (15.9% of total variation)
PC1 (45.7% of total variation)
T
Sal
DON
DOC
B12
NO_3^-
HPO_4^{2-}
SiO_4^{4-}
NH_4^+
NO_2^-

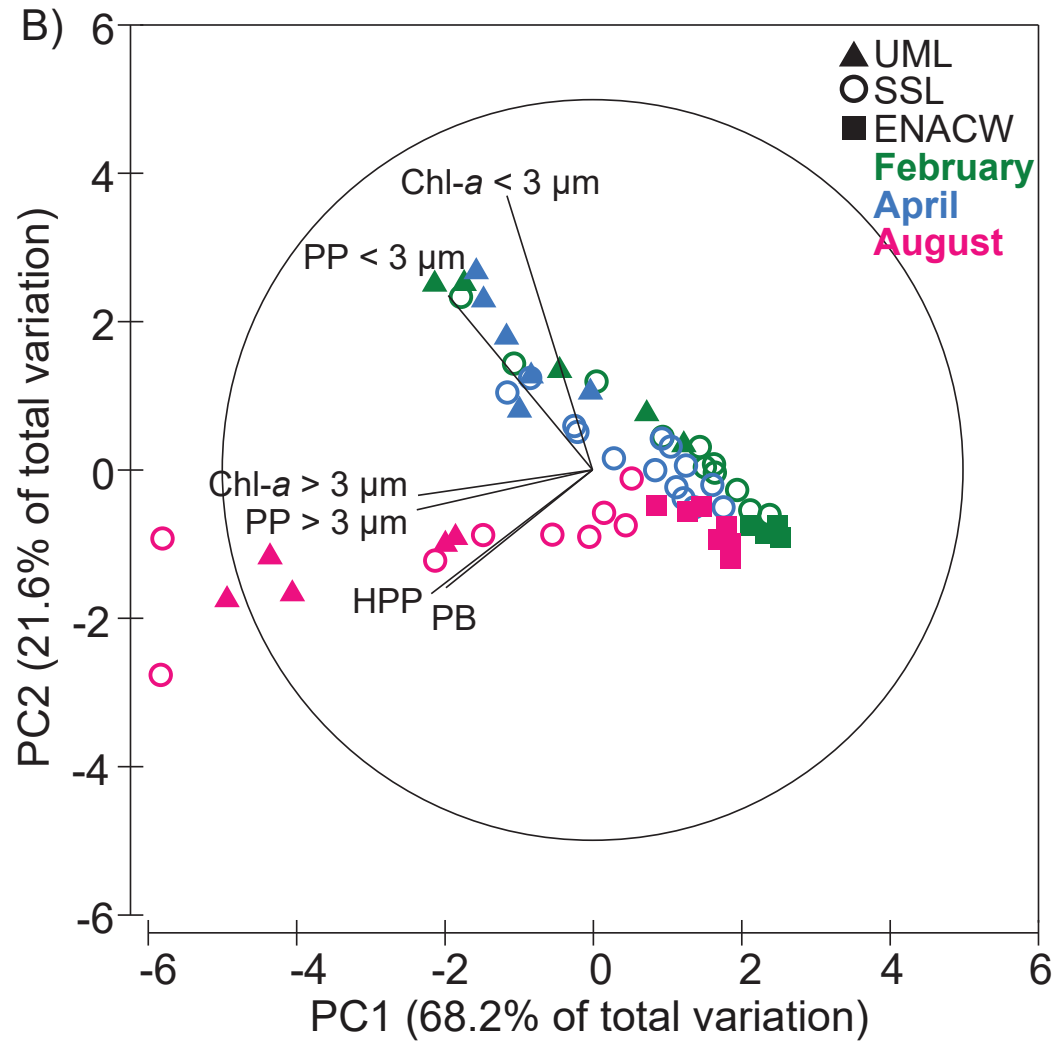
B)
UML
SSL
ENACW
February
April
August
Chl-a < 3 µm
PP < 3 µm
Chl-a > 3 µm
PP > 3 µm
HPP
PB
PC2 (21.6% of total variation)
PC1 (68.2% of total variation)

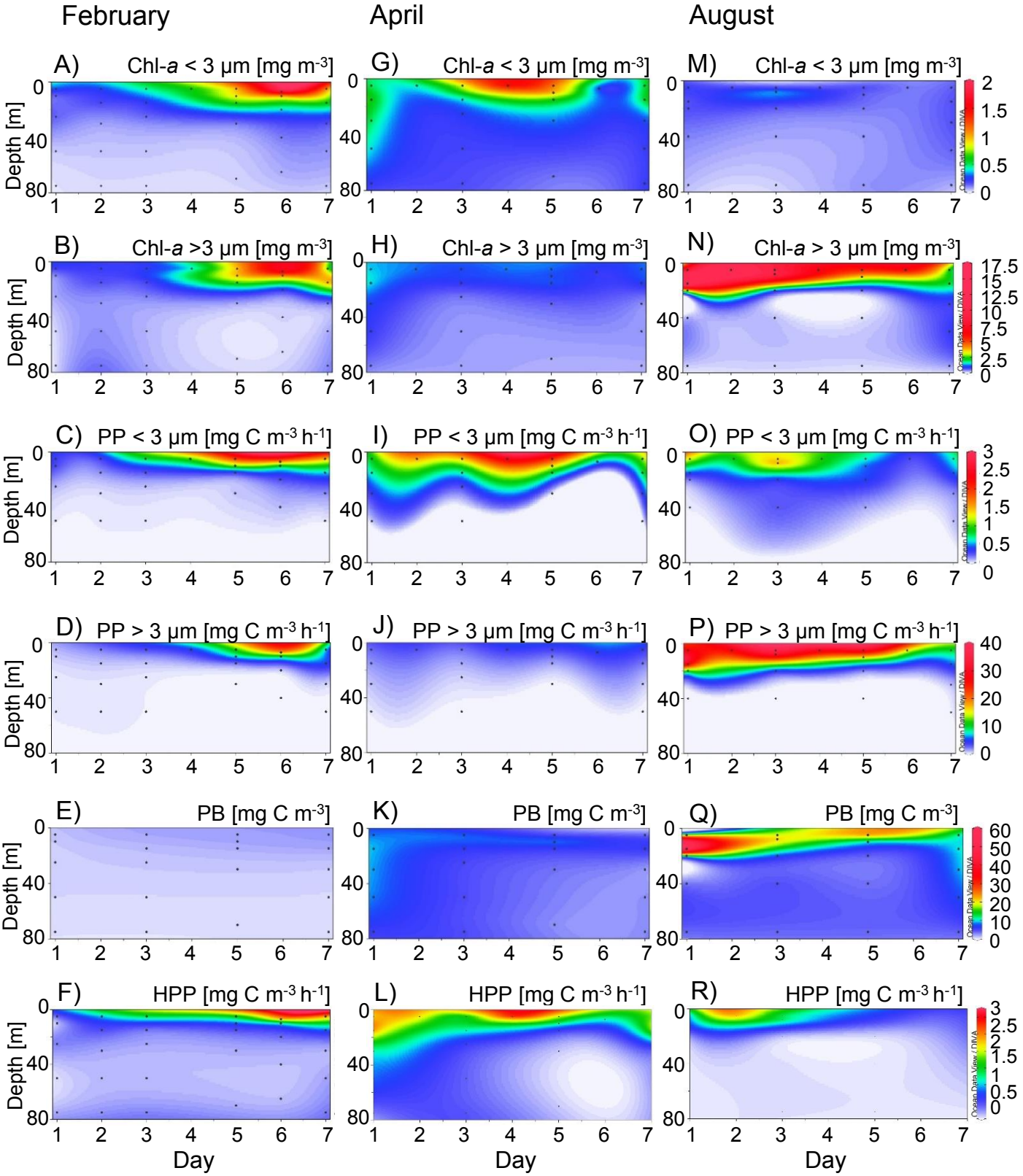
February
April
August
A) Chl-a < 3 µm [mg m-3]
G) Chl-a < 3 µm [mg m-3]
M) Chl-a < 3 µm [mg m-3]
B) Chl-a >3 µm [mg m-3]
H) Chl-a > 3 µm [mg m-3]
N) Chl-a > 3 µm [mg m-3]
C) PP < 3 µm [mg C m-3 h-1]
I) PP < 3 µm [mg C m-3 h-1]
O) PP < 3 µm [mg C m-3 h-1]
D) PP > 3 µm [mg C m-3 h-1]
J) PP > 3 µm [mg C m-3 h-1]
P) PP > 3 µm [mg C m-3 h-1]
E) PB [mg C m-3]
K) PB [mg C m-3]
Q) PB [mg C m-3]
F) HPP [mg C m-3 h-1]
L) HPP [mg C m-3 h-1]
R) HPP [mg C m-3 h-1]
Depth [m]
Day
Ocean Data View / DIVA

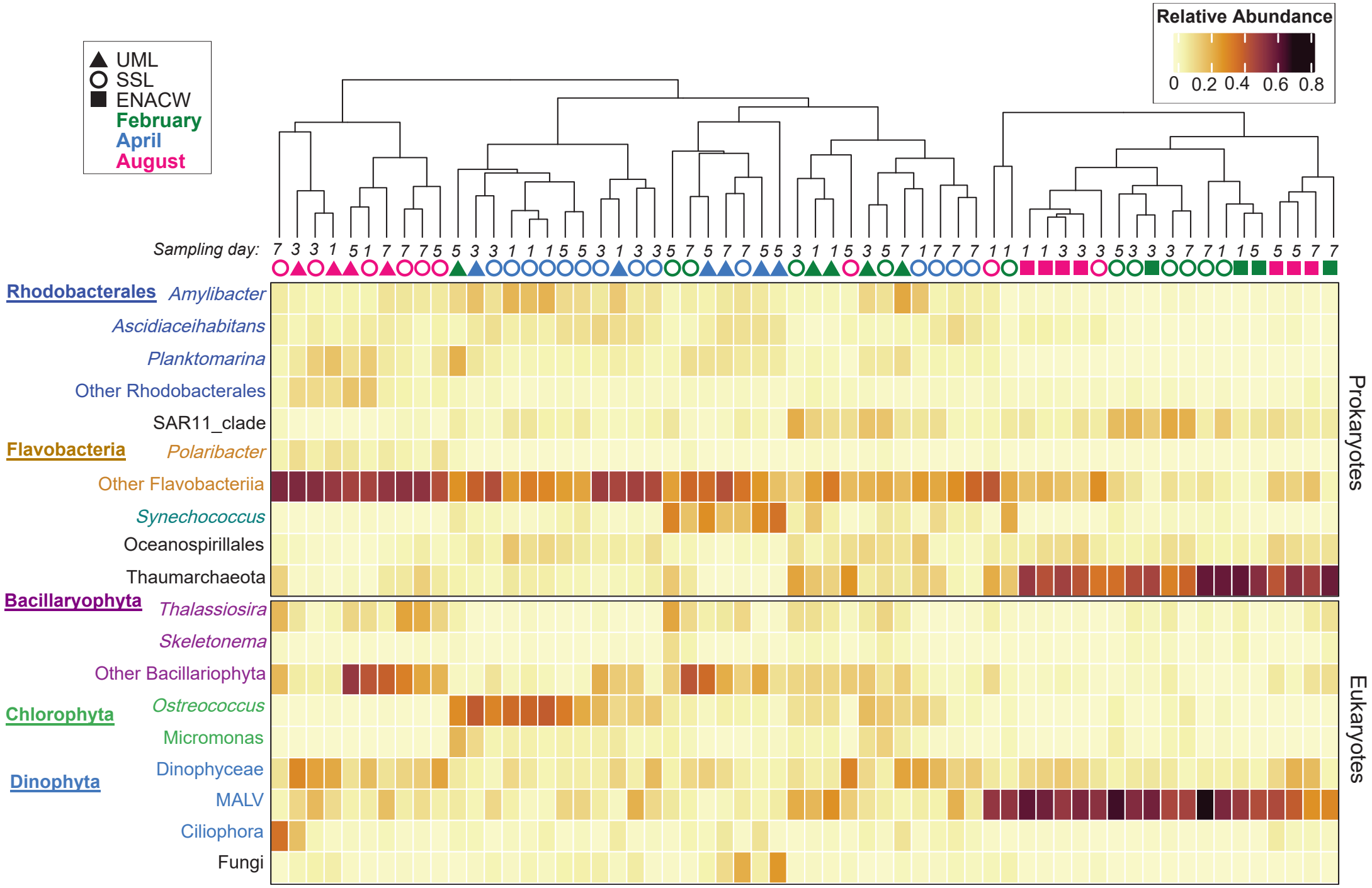
UML
SSL
ENACW
February
April
August
Relative Abundance
0 0.2 0.4 0.6 0.8
Sampling day:
7 3 3 1 5 1 7 7 7 5 5 3 3 1 1 1 5 5 3 1 3 3 5 7 5 7 7 5 5 3 1 1 5 3 5 7 1 7 7 7 1 1 1 1 3 3 3 5 3 3 3 7 7 1 1 5 5 5 7 7
Rhodobacterales
Amylibacter
Ascidiaceihabitans
Planktomarina
Other Rhodobacterales
SAR11_clade
Flavobacteria
Polaribacter
Other Flavobacteriia
Synechococcus
Oceanospirillales
Thaumarchaeota
Bacillaryophyta
Thalassiosira
Skeletonema
Other Bacillariophyta
Chlorophyta
Ostreococcus
Micromonas
Dinophyta
Dinophyceae
MALV
Ciliophora
Fungi
Prokaryotes
Eukaryotes

Figure 7

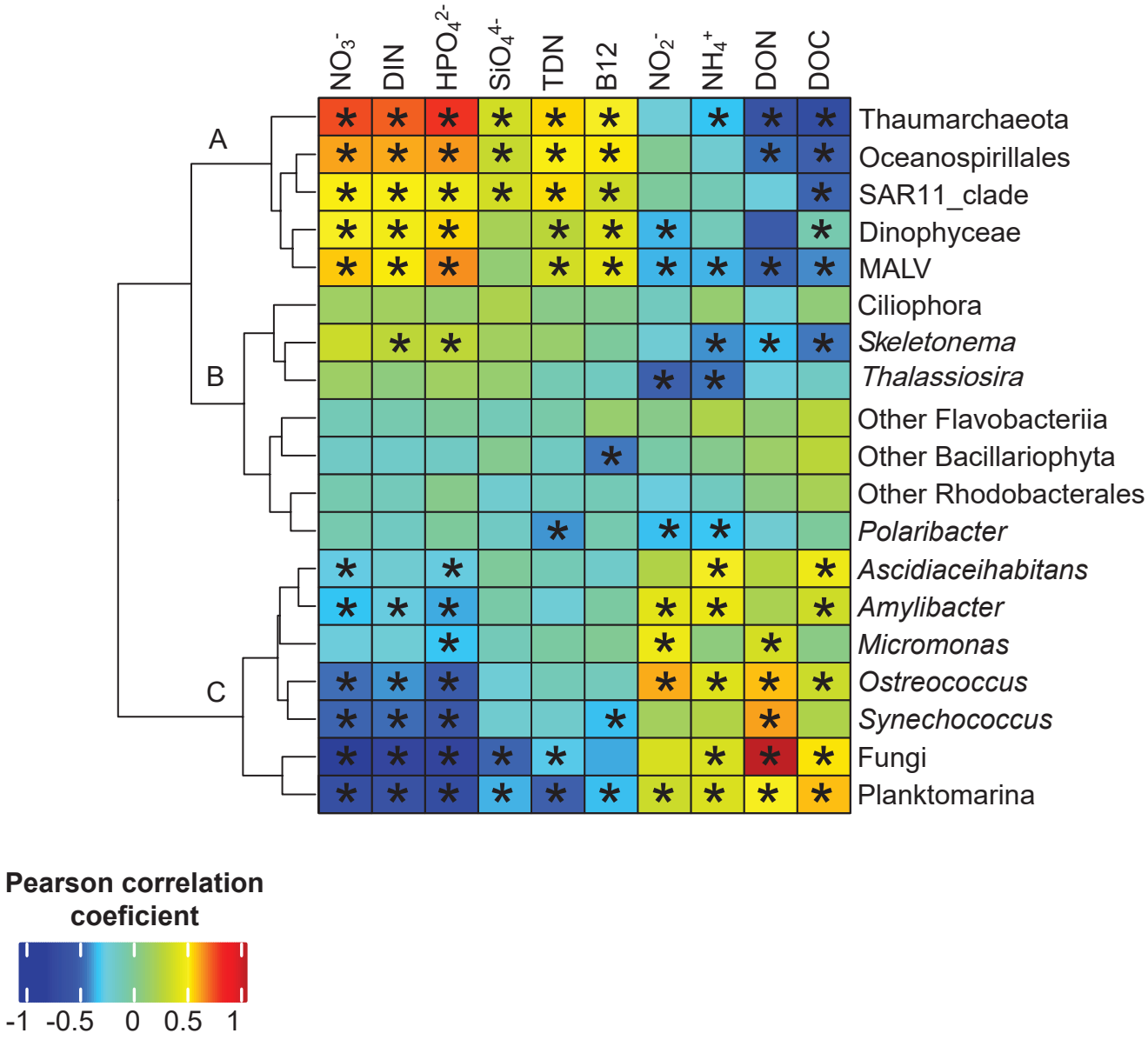
NO_3^-
DIN
HPO_4^{2-}
SiO_4^{4-}
TDN
B12
NO_2^-
NH_4^+
DON
DOC
A
B
C
Thaumarchaeota
Oceanospirillales
SAR11_clade
Dinophyceae
MALV
Ciliophora
Skeletonema
Thalassiosira
Other Flavobacteriia
Other Bacillariophyta
Other Rhodobacterales
Polaribacter
Ascidiaceihabitans
Amylibacter
Micromonas
Ostreococcus
Synechococcus
Fungi
Planktomarina
Pearson correlation coeficient
-1 -0.5 0 0.5 1

Figure 9

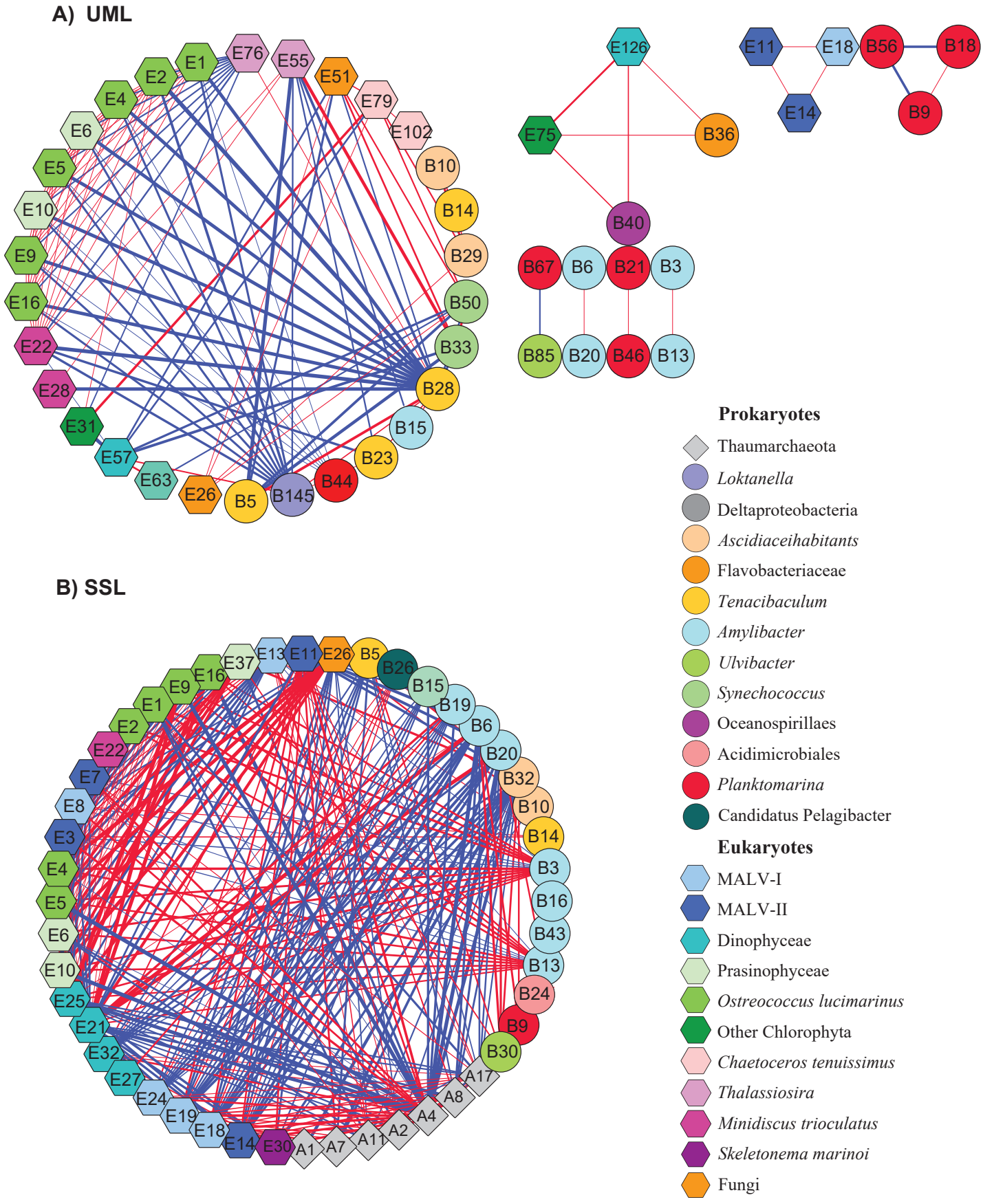
A) UML
E1
E76
E55
E51
E79
E102
E2
E4
E6
E5
E10
E9
E16
E22
E28
E31
E57
E63
E26
B5
B145
B44
B23
B15
B28
B33
B50
B29
B14
B10
E126
E75
B36
B40
B67
B6
B21
B3
B85
B20
B46
B13
E11
E18
B56
B18
E14
B9
B) SSL
E37
E13
E11
E26
B5
B26
B15
B19
B6
B20
B32
B10
B14
B3
B16
B43
B13
B24
B9
B30
A17
A8
A4
A2
A11
A7
A1
E30
E14
E18
E19
E24
E27
E32
E21
E25
E10
E6
E5
E4
E3
E8
E7
E22
E2
E1
E9
E16
Prokaryotes
Thaumarchaeota
Loktanella
Deltaproteobacteria
Ascidiaceihabitants
Flavobacteriaceae
Tenacibaculum
Amylibacter
Ulvibacter
Synechococcus
Oceanospirillaes
Acidimicrobiales
Planktomarina
Candidatus Pelagibacter
Eukaryotes
MALV-I
MALV-II
Dinophyceae
Prasinophyceae
Ostreococcus lucimarinus
Other Chlorophyta
Chaetoceros tenuissimus
Thalassiosira
Minidiscus trioculatus
Skeletonema marinoi
Fungi

C) ENACW

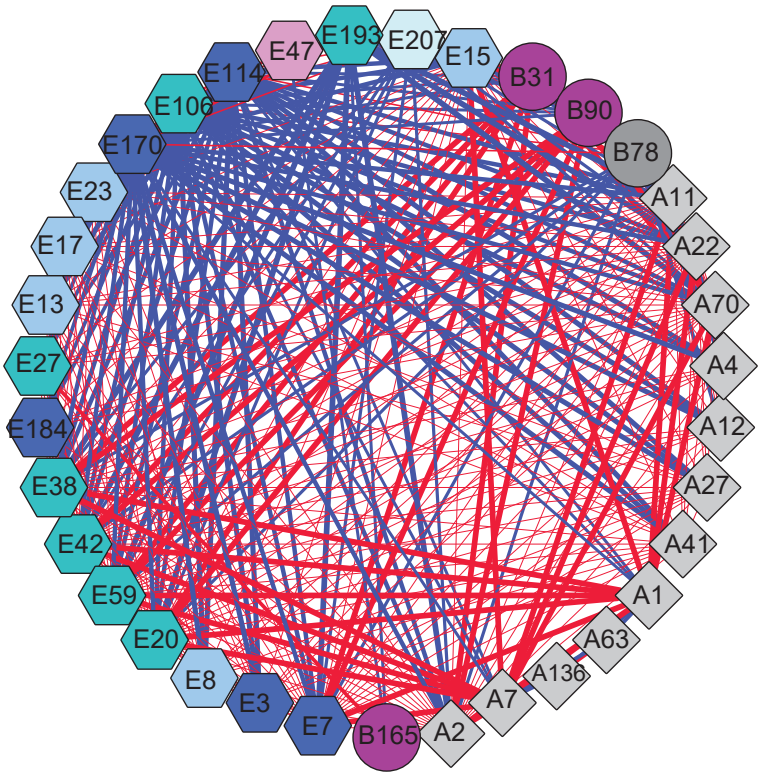
E47
E193
E207
E15
B31
B90
B78
A11
A22
A70
A4
A12
A27
A41
A1
A63
A136
A7
A2
B165
E7
E3
E8
E20
E59
E42
E38
E184
E27
E13
E17
E23
E170
E106
E114

ID	Taxa
A1	Thaumarchaeota
A11	Thaumarchaeota
A12	Thaumarchaeota
A136	Thaumarchaeota
A17	Thaumarchaeota
A2	Thaumarchaeota
A22	Thaumarchaeota
A27	Thaumarchaeota
A4	Thaumarchaeota
A41	Thaumarchaeota
A63	Thaumarchaeota
A7	Thaumarchaeota
A70	Thaumarchaeota
A8	Thaumarchaeota
B10	*Ascidiaceihabitans*
B13	*Amylibacter*
B14	*Tenacibaculum*
B145	*Loktanella*
B15	*Amylibacter*
B16	*Amylibacter*
B165	*Oceanospirillales*
B18	*Planktomarina*
B19	*Amylibacter*
B20	*Amylibacter*
B21	*Planktomarina*
B23	*Tenacibaculum*
B24	Acidimicrobiales
B26	*Pelagibacter*
B28	*Tenacibaculum*
B29	*Ascidiaceihabitans*
B3	*Amylibacter*
B30	*Ulvibacter*
B31	*Oceanospirillales*
B32	*Ascidiaceihabitans*
B33	*Synechococcus*
B36	Flavobacteriaceae
B40	*Oceanospirillales*
B43	*Amylibacter*
B44	*Planktomarina*
B46	*Planktomarina*
B5	*Tenacibaculum*
B50	*Synechococcus*
B56	*Planktomarina*
B6	*Amylibacter*
B67	*Planktomarina*
B78	Deltaproteobacteria
B85	*Ulvibacter*
B9	*Planktomarina*
B90	*Oceanospirillales*

ID	Taxa
E1	*Ostreococcus lucimarinus*
E10	Prasinophyceae
E102	*Chaetoceros tenuissimus*
E106	*Apicomplexa*
E11	MALV-II
E114	MALV-II
E126	Dinophyceae
E13	MALV-I
E14	MALV-II
E15	MALV-I
E16	*Ostreococcus lucimarinus*
E17	MALV-I
E170	MALV-II
E18	MALV-I
E184	MALV-II
E19	MALV-I
E193	*Apicomplexa*
E2	*Ostreococcus lucimarinus*
E20	Dinophyceae
E207	Filosa-Chlorarachnea
E21	Dinophyceae
E22	*Minidiscus trioculatus*
E23	MALV-I
E24	MALV-I
E25	*Balechina pachydermata*
E26	Exobasidiomycetes
E27	*Gyrodinium fusiforme*
E28	*Minidiscus trioculatus*
E3	MALV-II
E30	*Skeletonema marinoi*
E31	Pyramimonadales
E32	Dinophyceae
E37	Prasinophyceae
E38	*Gyrodinium spirale*
E4	*Ostreococcus lucimarinus*
E42	Thoracosphaeraceae
E47	*Thalassiosira*
E5	*Ostreococcus lucimarinus*
E51	Tremellomycetes
E55	*Thalassiosira anguste-lineata*
E57	*Prorocentrum*
E59	Thoracosphaeraceae
E6	Prasinophyceae
E63	Prorocentrum
E7	MALV-II
E75	*Botryococcus braunii*
E76	*Thalassiosira pseudonana*
E79	*Chaetoceros tenuissimus*
E8	MALV-I
E9	*Ostreococcus lucimarinus*

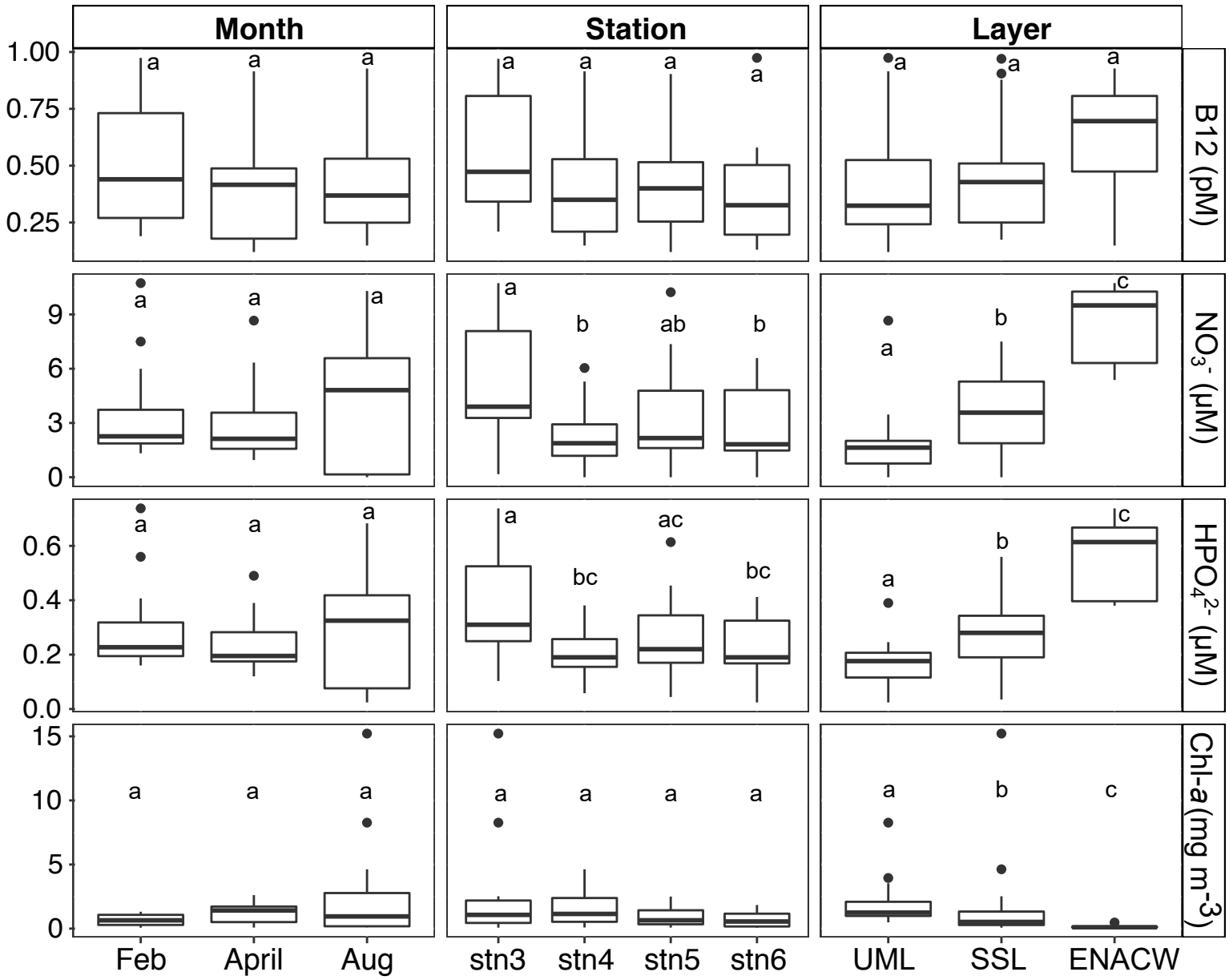
Month
Station
Layer
B12 (pM)
NO3- (µM)
HPO42- (µM)
Chl-a (mg m-3)
Feb
April
Aug
stn3
stn4
stn5
stn6
UML
SSL
ENACW

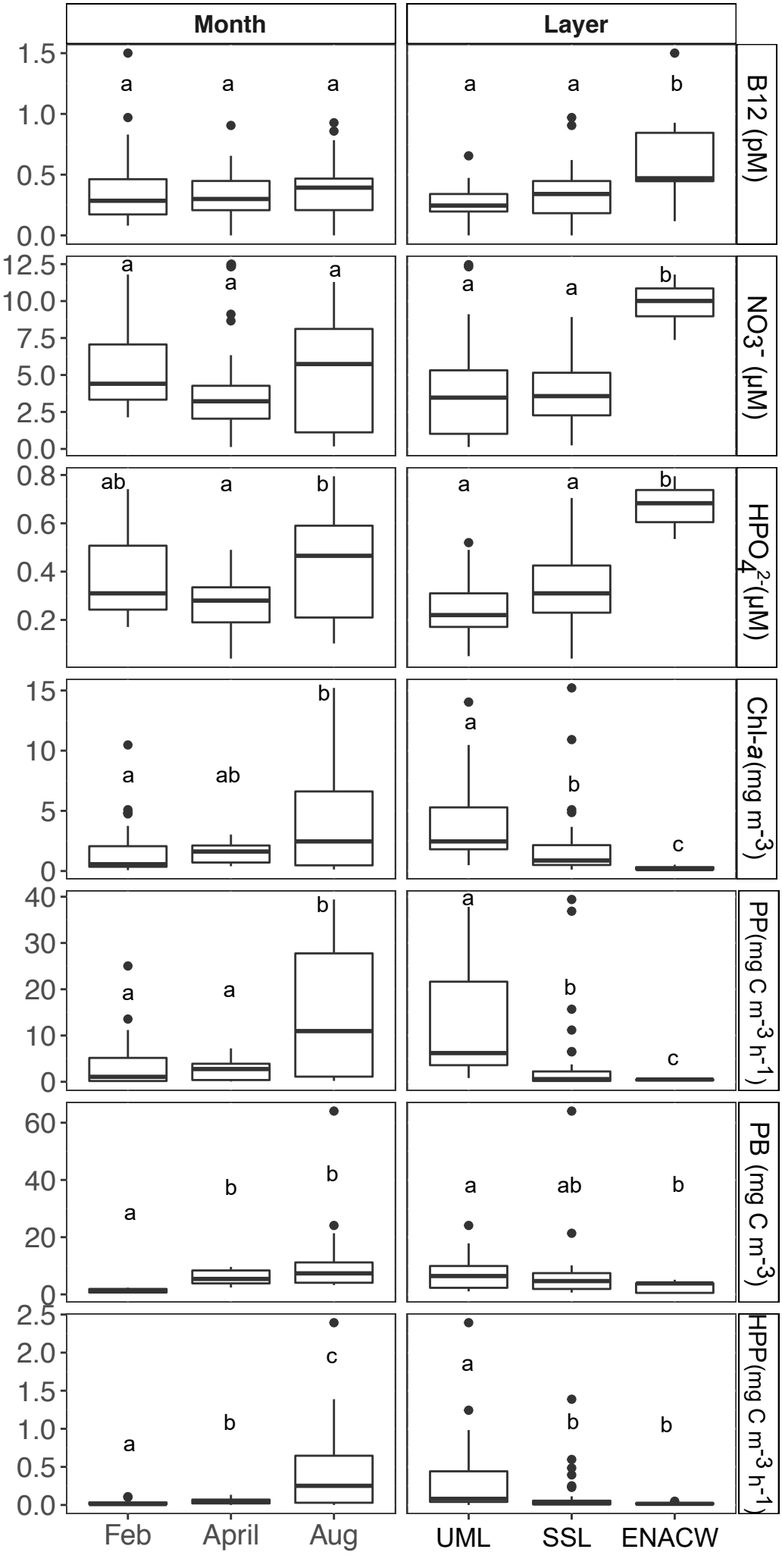
Month
Layer
B12 (pM)
NO3- (µM)
HPO4 2- (µM)
Chl-a (mg m-3)
PP (mg C m-3 h-1)
PB (mg C m-3)
HPP (mg C m-3 h-1)
Feb
April
Aug
UML
SSL
ENACW

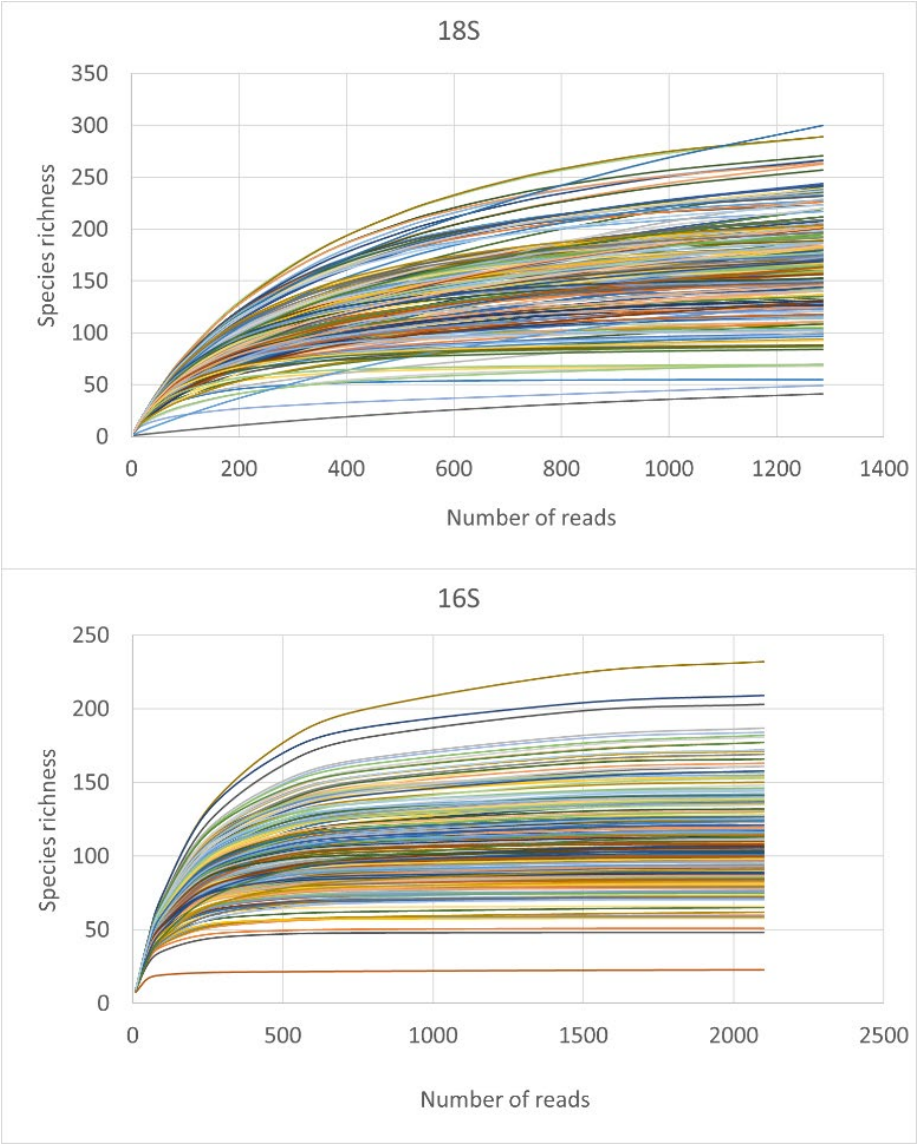
18S
Species richness
350
300
250
200
150
100
50
0
0
200
400
600
800
1000
1200
1400
Number of reads
16S
Species richness
250
200
150
100
50
0
0
500
1000
1500
2000
2500
Number of reads